FACULTY OF MEDICINE AND HEALTH SCIENCES

MRI changes after proton or photon radiotherapy for primary paediatric CNS tumours

Lore Vermeulen
Student number: 01806099

Supervisor: Prof. Dr. Tom Boterberg

A dissertation submitted to Ghent University in partial fulfilment of the requirements for the degree of Master of Medicine in Medicine

Academic year: 2022 – 2023

GHENT UNIVERSITY

Date 14/11/2022

Lore Vermeulen

Prof. Dr. T. Boterberg

ACKNOWLEDGEMENTS

Over the past two years, I have worked hard on this master's thesis. Its realisation would not have been possible without the help of a number of people whom I would like to thank.

I would like to thank my supervisor Prof. Dr. Tom Boterberg for his contribution to my work, his knowledge and critical assessments.

Furthermore, I would like to thank my parents and friends who have supported me during this intense period. In particular, Ancy Leroy and Jens Van de Velde for proofreading my text.

ABBREVIATIONS

ADC	Apparent diffusion coefficient
AT/RT	Atypical teratoid/rhabdoid tumour
CMB	Cerebral microbleed
CNS	Central nervous system
CSI	Craniospinal irradiation
CT	Computed tomography
CTCAE	Common Terminology Criteria for Adverse Events
CVA	Cerebrovascular accident
$D_{50\%}$	Mean dose to 50% of the irradiated volume
D_{max}	Maximum dose
DTI	Diffusion tensor imaging
DWI	Diffusion-weighted imaging
EPTN	European Particle Therapy Network
FA	Fractional anisotropy
FLAIR	Fluid attenuation inversion recovery
GTR	Gross total resection
Gy	Gray
IDH	Isocitrate dehydrogenase
IMPT	Intensity-modulated proton therapy
LET	Linear energy transfer
LET_d	Dose averaged linear energy transfer
LET_t	Track averaged linear energy transfer
LGG	Low-grade glioma
LQ	Linear quadratic

MRI	Magnetic resonance imaging
MRS	Magnetic resonance spectroscopy
MTR	Magnetization transfer ratio
OAR	Organ at risk
PBS	Pencil beam scanning
PNET	Primitive neuroectodermal tumour
PS	Passive scattering
PsP	Pseudoprogression
PTV	Planning target volume
PWI	Perfusion-weighted imaging
QUANTEC	Quantitative Analysis of Normal Tissue Effects in the Clinic
RBE	Relative biological effectiveness
$RBE_{1.1}$	Relative biological effectiveness of 1.1
RICE	Radiation-induced contrast enhancement
RN	Radiation necrosis
RT	Radiotherapy
SOBP	Spread-out Bragg peak
TIA	Transient ischemic attack
WHO	World health organisation

TABLE OF CONTENTS

Abstract (EN) 1
Abstract (NL) 2
1 Introduction 3
1.1 Imaging 3
1.2 Central nervous system tumours 4
1.2.1 Glioma 5
1.2.1.1 Astrocytoma 5
1.2.1.2 Ependymoma 6
1.2.1.3 Oligodendroglioma 6
1.2.2 Embryonal tumours 7
1.2.2.1 Medulloblastoma 7
1.2.2.2 Other embryonal tumours 7
1.2.3 Craniopharyngioma 8
1.2.4 Neurocytoma 8
1.2.5 Meningioma 8
1.3 Radiotherapy 9
1.3.1 Photon therapy 9
1.3.2 Proton therapy 9
1.3.3 Delivery techniques 11
1.3.3.1 Passive scattering 11
1.3.3.2 Pencil beam scanning 12
1.3.3.3 Intensity-modulated proton therapy 12
1.3.4 General principles and terminology 12
1.3.4.1 α/β ratio 12
1.3.4.2 Relative biological effectiveness 13
1.3.4.3 Linear energy transfer 14
1.3.5 Reimbursement in Belgium 14
1.4 Aim of the study 15
2 Methods 16
2.1 Pubmed 16
2.2 Embase 17
2.3 Screening 17
3 Results 19
4 Discussion 41
4.1 Imaging changes 41

4.1.1 Pseudoprogression 41
4.1.2 Radiation necrosis 41
4.1.3 Brainstem injury 42
4.2 Symptomatic versus asymptomatic 42
4.3 Radiotherapy 43
4.3.1 Proton versus photon radiotherapy 43
4.3.2 Delivery technique 43
4.3.3 Radiation dose 44
4.3.3.1 Physical dose 44
4.3.3.2 Biological dose 44
4.4 Adjuvant treatment 45
4.4.1 Surgery 45
4.4.2 Chemotherapy 46
4.5 Patient characteristics 46
4.5.1 Tumour 46
4.5.2 Age 47
4.5.3 Individual radiosensitivity 48
4.6 Limitations of the clinical studies 48
4.7 Limitations to this literature research 49
5 Conclusion and perspectives 50
6 References 51
Supplementary .....

Abstract (EN)

Introduction: Central nervous system (CNS) tumours are the most common solid tumours in children. Radiotherapy (RT) is an essential treatment modality to improve local control. Proton therapy is increasingly used in children as it reduces the total dose to surrounding normal tissue. However, unanticipated toxicities are reported. Moreover, published data suggests a putative higher risk of imaging changes but the significance of these changes is unknown. Therefore, we investigated magnetic resonance imaging (MRI) changes after proton or photon RT for primary paediatric CNS tumours. The aim of this narrative review is to provide an overview and critical assessment of the published literature.

Methods: A narrative review was performed through database searching. The search strategy was conducted in PubMed and Embase. 53 records were included in the final data analysis.

Results: Several studies describe the occurrence of imaging changes, such as pseudoprogression (PsP) and radiation necrosis (RN). The reported incidence of imaging changes ranged from 5% to 47%. Although most of these imaging changes remained asymptomatic, some of them caused symptoms (2.4% to 24%). Several patient- and treatment-related factors were indicated as significant risk factors for the development of imaging changes. These patient-related factors include tumour histology, tumour location, patient's age and individual radiosensitivity, whereas the treatment-related factors include radiotherapy characteristics, surgery and chemotherapy. Finally, studies comparing proton and photon treated children, indicated an increased risk of imaging changes after proton RT.

Conclusion: RN is the most feared treatment complication after RT. Especially RN of the brainstem is of concern as it is associated with a mortality risk. Our main finding is that the development of MRI changes is multifactorial. Both patient- and treatment-related factors should be considered to minimise the risk of imaging changes. Further research is recommended to better understand the impact of these individual factors and their interactions. Finally, further research should investigate whether long-term advantages of proton RT outweigh the risks of complications.

Abstract (NL)

Introductie: Tumoren van het centraal zenuwstelsel (CZS) zijn de meest voorkomende vast weefsel tumoren bij kinderen. Radiotherapie (RT) is een essentiële behandelingsmethode om de lokale controle van deze tumoren te verbeteren. Proton therapie wordt steeds vaker gebruikt bij kinderen omdat het de totale dosis op de hersenen vermindert. In de literatuur worden echter onverwachte neveneffecten gerapporteerd. Bovendien suggereren gepubliceerde gegevens een mogelijk hoger risico op beeldvormingsveranderingen na proton therapie. De betekenis van deze beeldvormingsveranderingen is echter onbekend. Daarom onderzochten wij MRI veranderingen na proton of foton therapie voor primaire pediatrische CZS tumoren. Het doel van deze review is een overzicht en kritische beoordeling te geven van de gepubliceerde literatuur.

Methodologie: De zoekstrategie werd uitgevoerd in PubMed en Embase. 53 records werden opgenomen in de literatuur analyse.

Resultaten: Verschillende studies beschrijven het optreden van beeldvormingsveranderingen, zoals pseudoprogressie en radionecrose. De gerapporteerde incidentie varieerde van 5% tot 47%. Hoewel de meeste beeldvormingsveranderingen asymptomatisch bleven, veroorzaakten sommige ervan symptomen (2,4% tot 24%). Verschillende patiënt- en behandeling- gerelateerde factoren werden aangegeven als significante risicofactoren voor de ontwikkeling van beeldvormingsveranderingen. Tot deze patiënt-gerelateerde factoren behoren de tumor histologie, de tumor locatie, de leeftijd van de patiënt en de individuele stralingsgevoeligheid. Tot de behandeling-gerelateerde factoren behoren radiotherapeutische karakteristieken, chirurgie en chemotherapie. Ten slotte werd vastgesteld dat er een hoger risico is op beeldvormingsveranderingen na proton therapie dan na foton therapie.

Conclusie: Radionecrose is de meest gevreesde behandelingscomplicatie na RT. Vooral radionecrose van de hersenstam is van belang omdat het gepaard gaat met risico op sterfte. Onze belangrijkste bevinding is dat de ontwikkeling van MRI veranderingen multifactorieel is. Er moet rekening gehouden worden met zowel patiënt- als behandeling-gerelateerde factoren om het risico op beeldvormingsveranderingen te minimaliseren. Verder onderzoek is aanbevolen om het effect van deze afzonderlijke factoren en hun interacties beter te begrijpen. Ten slotte moet verder onderzoek nagaan of de voordelen van proton therapie op lange termijn opwegen tegen de risico's op complicaties.

1 Introduction

Central nervous system (CNS) tumours are the most common solid tumours in children. Radiotherapy (RT) is an essential treatment modality to improve local control. Proton therapy is increasingly used in children as it reduces the total dose to surrounding normal tissue. However, unanticipated toxicities are reported. Moreover, published data suggests a putative higher risk of imaging changes but the significance of these changes is unknown. Therefore, we investigated magnetic resonance imaging (MRI) changes after proton or photon RT for primary paediatric CNS tumours.

1.1 Imaging

In neuro-oncology, imaging is essential for diagnosis, treatment planning and follow-up (1). The preferred imaging modality to evaluate CNS tumours is MRI. MRI provides excellent soft tissue contrast, enabling the differentiation of tumours from normal tissue and inflammatory reactions, especially when combining morphological with functional MRI techniques. The most common morphological MRI techniques are T1 and T2 weighted sequences. T1 weighted sequences represent more closely the anatomy, while T2 weighted sequences are more useful to detect pathological changes. Another sequence called FLAIR, removes the high signal from cerebrospinal fluid in brain images. This is most useful to detect subtle abnormalities in areas close to cerebrospinal fluid. These morphological MRI sequences are shown in Figure 1.

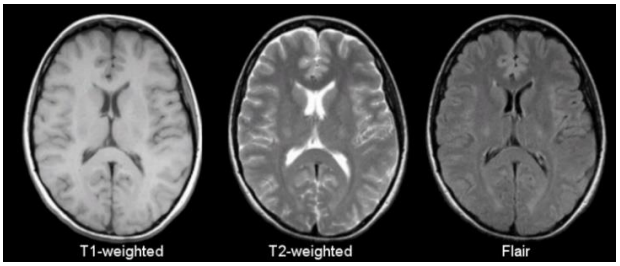

Fig. 1 Example of morphological MRI sequences. From left to right: T1, T2, FLAIR (2).

Functional MRI techniques such as diffusion, perfusion and spectroscopy enable microstructural evaluation of tissue. Diffusion-weighted imaging (DWI) is obtained by measuring water molecule movements. The extent of these movements is determined by the cellular density of the tissue. Based on DWI, the apparent diffusion coefficient (ADC) can be calculated. This coefficient represents the diffusion within the tissue. For example, high cellular density causes less water molecule movements, resulting in a high signal on DWI and a low ADC value. Diffusion tensor

imaging (DTI) measures the direction of water molecule movements to estimate the axonal organisation of the brain. Based on DTI, the fractional anisotropy (FA) can be calculated. The FA value indicates the direction of diffusion. Perfusion-weighted imaging (PWI) provides information regarding tumour microcirculation. Magnetic resonance spectroscopy (MRS) identifies the presence of different metabolites within brain tissue. In brain tumours, progressive changes of multiple metabolites correlate with tumour grade.

In addition to its diagnostic role, MRI is also important in the follow-up of CNS tumours. MRI is used to monitor the outcome of treatment and radiation-induced brain toxicity. The recommendations for follow-up depend on the type of tumour and the response to treatment.

The use of computed tomography (CT) is limited in neuro-oncology since MRI offers superior tissue contrast. However, the initial diagnosis of a CNS tumour is often made on CT, especially in case of acute symptoms related to the mass effect of the tumour. Moreover, CT remains an important imaging modality to detect calcifications typically present in some brain tumours (1).

1.2 Central nervous system tumours

CNS tumours are the most common solid tumours in children (1). In 2020 the incidence rate in Belgian patients up to 20 years was 20.9/100,000 (3).

CNS tumours include several different types all requiring an individual approach. A complete overview of all CNS tumours is beyond the scope of this master's thesis. For a list of all CNS tumours, we refer to the WHO classification of 2021 (4). In this master's thesis, the WHO classification of 2016 will be applied to allow the interpretation of published literature. Important changes in the current classification, relevant for this master's thesis, will be mentioned.

Astrocytomas (e.g., pilocytic, diffuse astrocytoma) and medulloblastomas are the most common paediatric CNS tumours. Neurocytomas are least common in children. Further details of the distribution are shown in Figure 2. For most tumours there is no gender predominance. Only embryonal tumours and germinal cell tumours are more common in males than in females (5). In terms of prognosis, the distinction between benign and malignant tumours is sometimes less relevant than for other tumours. Benign CNS tumours can also have a poor prognosis depending on their localisation.

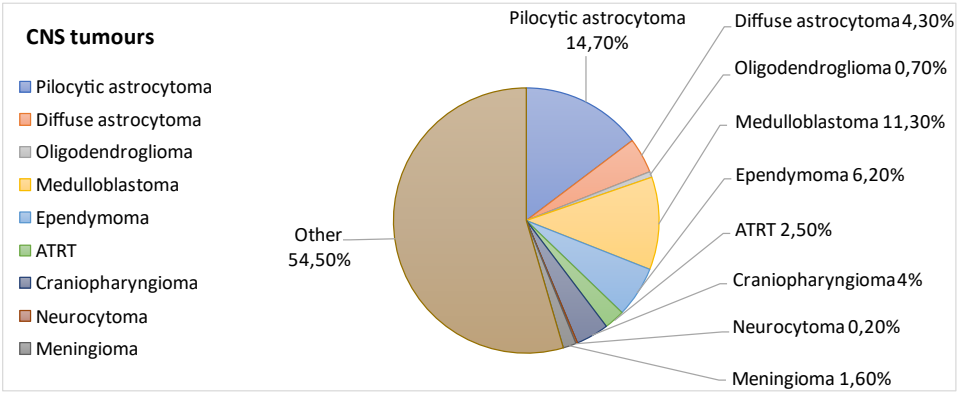

Fig. 2 Distribution of paediatric CNS tumours adapted from (5).

1.2.1 Glioma

Gliomas are neuroepithelial tumours arising from the supporting cells (glial cells) of the central nervous system. There are 3 types of glial cells: astrocytes, ependymal cells and oligodendrocytes. Tumours arising in these tissues are named after their origin (1). Their new WHO 2021 classification is shown in Table S1 (supplementary data). A simplified scheme of the management of gliomas is shown in Figure 3.

1.2.1.1 Astrocytoma

Astrocytomas can be divided in low- and high-grade tumours. Low-grade tumours include the pilocytic (WHO grade I) and diffuse (WHO grade II) astrocytomas. Pilocytic astrocytomas are named after the hair-like or piloid appearance of the cells. They generally occur as well circumscribed tumours mainly located in the posterior fossa (60%) or optic pathways (30%). Optic pathway pilocytic astrocytoma may be associated with neurofibromatosis type 1. Pilocytic astrocytomas often have cystic and solid components which causes a heterogeneous appearance on MRI. T1 with gadolinium contrast is the preferred imaging modality. The low to moderate cellular density of the tumour causes a low signal on DWI.

Diffuse astrocytomas have a more aggressive growth pattern. They mainly occur in the supratentorial region. For these tumours T2/FLAIR is the preferred imaging modality. Over time, malignant progression to high-grade astrocytoma may occur. High-grade astrocytomas can also develop as primary tumours, without a low-grade predecessor. These high-grade tumours include anaplastic astrocytomas (WHO grade III) and glioblastomas (WHO grade IV). These are less common in paediatric patients. They mainly occur in the supratentorial region or the cerebral lobes. Maximal resection remains the optimal treatment approach for astrocytomas. Depending on the WHO grade, adjuvant therapy is applied. Details of the management are shown in Figure 3 (1).

1.2.1.2 Ependymoma

Ependymomas arise from ependymal cells lining the ventricles and spinal canal. In children, most of the ependymomas have an intracranial presentation. They mainly occur in the posterior fossa (⅔) or the supratentorial region (⅓). Most posterior fossa tumours present in the fourth ventricle. They are characterised by an extension through the ventricular foramina and an involvement of the cerebello-pontine angle. CT demonstrates an isodense to hyperdense lesion often associated with calcifications or haemorrhage. MRI typically shows a T1 hypointense lesion with heterogenous contrast enhancement and a T2 hyperintensity. The low to moderate cellular density of the tumour causes a low signal on DWI. An MRI spine is a crucial investigation to exclude leptomeningeal dissemination, together with a lumbar puncture before or at least 14 days after surgery. Treatment involves gross total resection (GTR) followed by adjuvant focal RT. Chemotherapy is currently investigated to delay or avoid RT in very young children or as adjuvant therapy after RT (1).

1.2.1.3 Oligodendroglioma

Oligodendrogliomas (WHO grade II or III) are similar to diffuse astrocytomas in terms of growth pattern, location, preferred imaging modality and treatment. These characteristics will not be repeated. Cystic degeneration and calcification are common features on imaging. 1p19q codeletion is a key feature for their diagnosis (1).

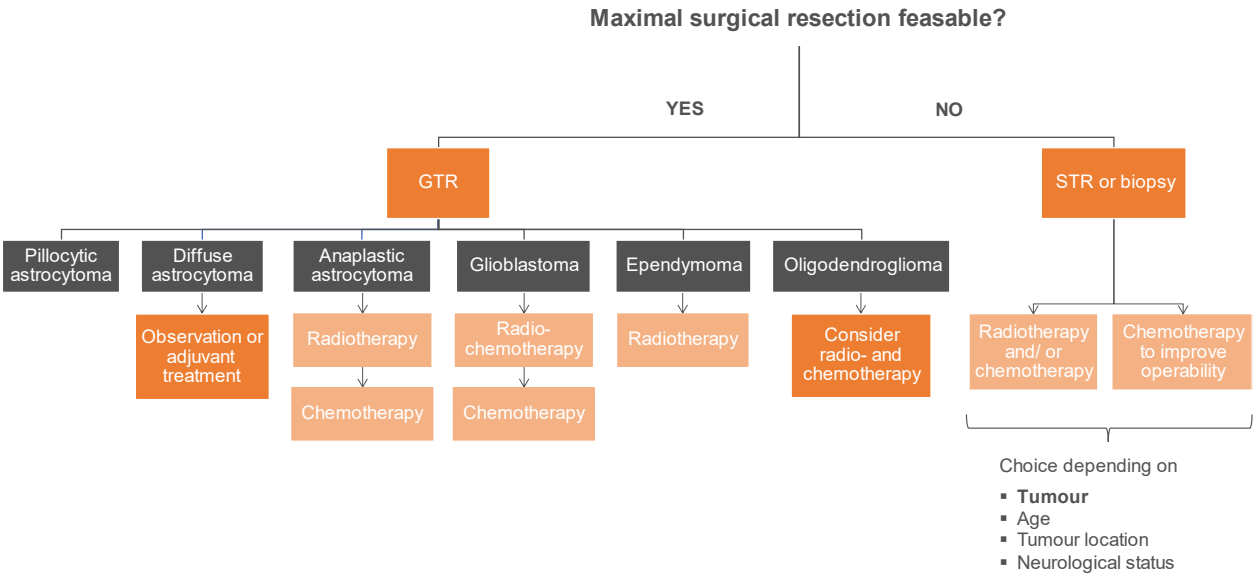

Fig. 3 Simplified scheme of the management of gliomas: (grey) gliomas, (orange) therapy, (faded orange) adjuvant therapy.
Abbreviations: GTR, gross total resection; STR, subtotal resection

1.2.2 Embryonal tumours

1.2.2.1 Medulloblastoma

Medulloblastomas arise from cerebellar stem cells and have a high cellular density. These embryonal tumours are mainly located in the posterior fossa. CT shows a hypodense mass in the posterior fossa, possibly associated with an obstructive hydrocephalus. Medulloblastomas appear hyperdense on CT imaging after contrast application. MRI shows a homogeneous contrast enhancement in the majority of cases. The high cellular density causes a high signal on DWI. This is an important imaging feature, useful in differential diagnosis with other tumours localized in the same area (i.e. pilocytic astrocytoma, ependymoma) and in the postoperative setting to determine the extent of resection.

The treatment of medulloblastomas consists of a combination of surgery, chemotherapy and radiotherapy. The purpose of surgery is to obtain a maximal resection, relief of symptoms and a tissue specimen for histopathological and molecular analysis. Postoperative RT involves craniospinal irradiation (CSI) followed by a boost on the tumour bed (including a possible tumour remnant). The dose schedule and chemotherapy regimen depend on the risk stratification (Table S2) of the tumour. Although the cure rate is relatively high, long-term side effects including neurocognitive impairment and endocrine failure occur in some cases. These neurocognitive sequelae are more pronounced in younger children since the developing brain is more sensitive to radiation-induced toxicity (1).

1.2.2.2 Other embryonal tumours

Besides medulloblastoma, there are several other embryonal tumours including the atypical teratoid/rhabdoid tumour (AT/RT) (WHO grade IV). This malignant tumour consists of rhabdoid, neuroepithelial, epithelial and mesenchymal cells. AT/RTs mainly occur in the posterior fossa or supratentorial region. Imaging findings are comparable to other embryonal tumours. There is no consensus for an optimal approach. Current treatment protocols include a combination of surgery, high dose chemotherapy and radiotherapy. The use of RT depends on the metastatic status of the tumour and the age of the patient. In metastatic AT/RT, RT involves craniospinal irradiation followed by a boost dose. In non-metastatic disease, only the tumour bed is irradiated. As AT/RTs typically occur in very young children, the use of RT should be considered carefully, but on the other hand, seems to be crucial in disease control. Given the poor prognosis, symptom control and palliative care are essential in the management of these tumours. In addition to AT/RTs, other very rare embryonal tumours include embryonal tumour with multilayered rosettes, embryonal tumour NOS and medulloepithelioma (1).

1.2.3 Craniopharyngioma

Craniopharyngiomas (WHO grade I) originate from the embryonal squamous cell remnants of the involuted Rathke's pouch. These neuroepithelial tumours are localized in the sellar region. This is close to sensitive brain structures such as the hypothalamus, the pituitary gland and the optic pathways. Therefore, the tumour has a variable clinical presentation depending on its extent and the affected surrounding structures. There are two pathological types: the papillary and adamantinomatous craniopharyngiomas. Adamantinomatous craniopharyngiomas are mainly seen in children. They usually have both cystic and solid components causing a heterogeneous appearance on MRI. The cysts can be hyperintense on T1 and T2 when they contain high-density fluid.

The management of craniopharyngiomas is complex and there is no evidence for an optimal approach. The current approach is based on the impairment of the hypothalamus. When the hypothalamus is not affected, a gross total resection is performed. However, when the hypothalamus is affected, this approach is not recommended due to the risk of severe damage with significant complications. In this case a subtotal resection with postoperative RT will be performed. In a craniopharyngioma, the cystic component can change (enlarge or reduce in volume) during RT. Therefore, regular imaging with CT or MRI is recommended. This monitoring is extremely important to adjust the RT plan if necessary, especially if proton RT is used (1).

1.2.4 Neurocytoma

Neurocytomas (WHO grade II) are extremely rare in children. These benign intracranial tumours are derived from neural cells. If feasible, GTR is the treatment of choice. The use of RT is not considered as standard of care (1).

1.2.5 Meningioma

Meningiomas originate from the meninges. Consequently, these tumours are mainly located in the convexity of the skull. Since the meninges consist of different layers and therefore different cell types, meningiomas can be divided into 15 subtypes (WHO grade I, II or III) (4). Meningiomas are benign tumours but may behave more aggressively in children than in adults. They are associated with genetic syndromes (e.g., neurofibromatosis type 2) or previous irradiation. MRI typically shows a T1 contrast enhancement and T2 hyperintensity. Dural attachment or "tail" is pathognomonic in adults but is less common in children. Frequent characteristics of paediatric meningiomas are cystic lesions and calcifications. CT is especially valuable to detect these calcifications or hyperostosis

caused by bone invasion. Treatment involves GTR. The use of RT is not considered as standard of care. It is only applied for inoperable, residual or recurrent disease (1).

1.3 Radiotherapy

There are three treatment modalities for CNS tumours: surgery, radiotherapy and chemotherapy. For surgery the balance between the benefits of complete resection and the risk of neurological damage must be considered (1). CNS tumours very rarely metastasize outside the central nervous system (5). Therefore, further local treatment with RT is a fundamental component to improve local control in the management of primary CNS tumours. The mechanism of action of RT is based on radiation-induced DNA damage, which leads to tumour cell death (6). However, it is not always possible to deliver lethal tumour doses because of radiation-induced toxicity to normal tissue. The brain contains several dose-limiting structures such as the brainstem, optic structures and hippocampus. They tolerate only a limited radiation dose, often lower than the dose needed to treat the tumour adequately. Before treatment planning, these structures are delineated as organs at risk (OAR). These OAR must be considered during treatment planning, keeping the dose they receive as low as possible and certainly within the known dose constraints.

1.3.1 Photon therapy

Photon therapy is considered as standard RT. Photons or x-rays are high energy electromagnetic radiation. The dose deposition is caused by secondary electrons generated during tissue interactions. The rapid increase in the number of these electrons results in a dose build-up. Therefore, depending on their energy, photons have a maximum dose deposition at a certain depth after entering the tissue. The transferred radiation dose then exponentially decreases while crossing the tissue. This results in additional dose to surrounding healthy tissue along the beam path in front of and behind the tumour (Fig. 4). In RT, cell death is caused by a combination of direct and indirect DNA damage. Direct DNA damage is caused by the irradiation (primary and secondary), whereas indirect damage is caused by free radicals generated during the interaction of the x-rays with water molecules. Therefore, the biological effect of photon therapy is more than only the physical effect of the used irradiation.

1.3.2 Proton therapy

Protons have different physical and radiobiological characteristics and therefore a different pattern of energy deposition and dose distribution than photons. Protons are positively charged particles.

While moving through tissue they interact with the atomic electrons. In each interaction, a limited amount of proton energy is transferred to the electron, causing excitation or ionisation. Due to multiple interactions the proton energy continuously decreases. This energy loss decreases the velocity of the protons. Decrease in velocity results in an increase of energy exchange because slower protons lose more energy due to a longer interaction with the electrons. The increasing energy loss with increasing depth results in a maximum dose deposition at the end of their trajectory, known as the Bragg peak. Behind the Bragg peak, contrary to photons, dose rapidly decreases to zero. The rate of dose reduction determines the distal dose fall-off. This physical characteristic allows to better confine the radiation dose to the tumour and to limit the dose in surrounding healthy tissue especially behind the tumour. Protons randomly interact with the atomic electrons. As a result, protons with the same energy stop at slightly different depths. This range straggling widens the Bragg-peak in depth and results in a range uncertainty at the distal end of the beam. The combination of several Bragg peaks from several beams with different energy levels results in a Spread-out Bragg peak (SOBP) (Fig. 4). This SOBP is required to cover a tumour volume.

The second mechanism of proton-tissue interaction is with the atomic nucleus. This interaction can have two consequences. When the proton conserves its energy during the nuclear interaction, the particle is deflected. These small-angle deflections affect the lateral margins of the beam. The area of rapid dose reduction at the lateral edge of the beam is called the penumbra. When the energy is not conserved, secondary particles are created. These particles reduce the primary proton fluence and can deliver their energy at a distance from the primary beam path (6, 7). Importantly, this lateral penumbra can be larger for protons than for photons, especially for low energy protons.

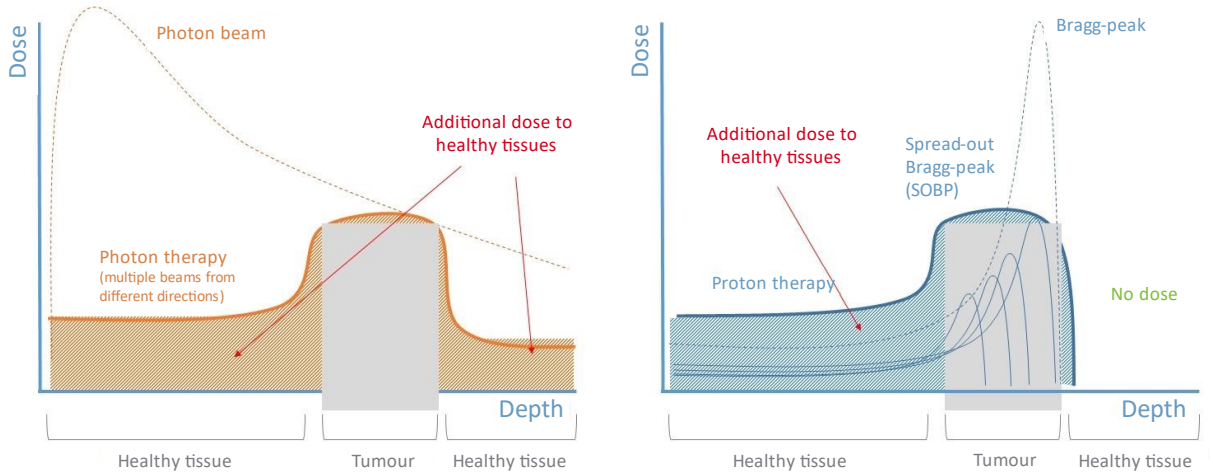

Fig. 4 Depth dose curve of a photon and proton beam adapted from (8).

1.3.3 Delivery techniques

Protons are accelerated in a cyclotron to obtain the required energy for therapeutic applications. The two major delivery techniques in proton therapy are passive scattering (PS) and pencil beam scanning (PBS) (Fig. 5). PS is the oldest modality, therefore most patients receiving proton therapy have been treated with this technique. Since PBS has significant dosimetric advantages compared to PS, current treatment facilities are increasingly using PBS (7). When interpreting published data, it is necessary to consider which delivery technique was used in the study.

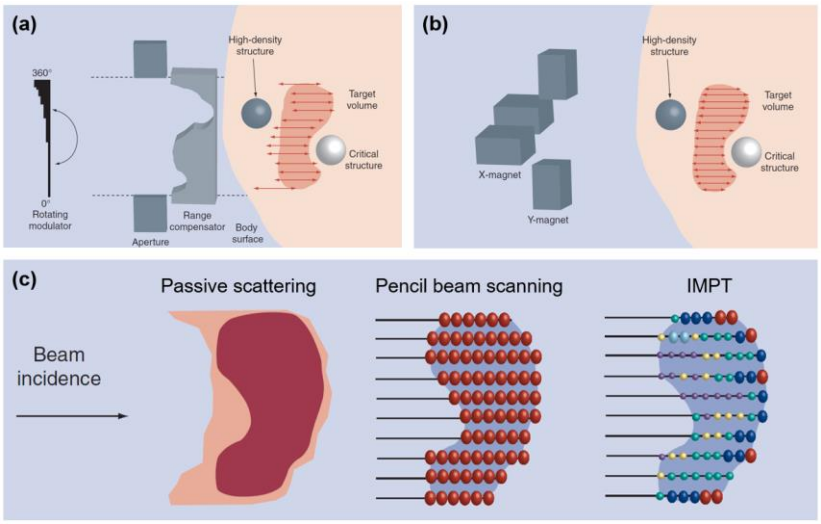

Fig. 5 Proton beam delivery techniques. Passive scattering (a); pencil beam scanning (b); dose distribution of passive scattering, pencil beam scanning and intensity modulated proton therapy (IMPT) (c) adapted from (7).

1.3.3.1 Passive scattering

In PS a combination of different methods is used to create a proton field that covers the target volume (Fig. 5a). By varying the beam energy with a range modulator, various pristine Bragg peaks are delivered. The combination of these pristine Bragg peaks results in a SOBP. The flat dose plateau of the SOBP results in a homogeneous dose distribution (Fig. 5c). To create a proton field that covers the target volume, the narrow proton beam is spread in the lateral dimension by a scattering system. Further shaping of this proton field is confined within the lateral extents of the target volume by the aperture. The distal end of the SOBP is placed at the distal end of the target volume by a range compensator. In this way, the protons stop at the right depth. Two PS techniques are possible: single and double scattering. In single scattering only one scatterer is used to achieve

a narrow treatment field. This is typically used in the treatment of small target volumes. In double scattering a second scatterer is added to further broaden the proton field (7).

1.3.3.2 Pencil beam scanning

The direction of a proton beam can be modified by magnetic fields. This feature is applied in PBS. In PBS two dipole magnets are used to adjust the vertical and horizontal direction of the beam (Fig. 5b). The penetration depth of the beam is controlled by varying the proton energy. This allows to scan the target volume spot by spot and layer by layer. Two PBS techniques are possible: spot and raster scanning. In spot scanning, the dose is delivered to one specific spot. Then the beam is turned off while the strength of the magnetic fields is changed to target the next spot. In raster scanning, an entire layer is irradiated line by line without turning off the beam. PBS can deliver a homogeneous or heterogeneous dose distribution (Fig. 5c). A homogeneous dose is obtained by irradiating each spot with the same proton intensity. A heterogeneous dose distribution is created by changing the intensity at specific positions in the target volume. This is also called intensity-modulated proton therapy (IMPT) which is described below (7).

1.3.3.3 Intensity-modulated proton therapy

In IMPT, changing the proton intensity at various positions creates a heterogeneous dose distribution (Fig. 5c). Multiple heterogeneous irradiation fields can approach the target volume from different directions. The combination of these fields results in the desired (homogeneous or heterogeneous) dose distribution. In IMPT the total dose to healthy tissue is limited along the beam path because the radiation source is coming from different directions. This allows more flexibility in avoiding critical structures (7). On the other hand, the total dose bath will increase.

1.3.4 General principles and terminology

1.3.4.1 α/β ratio

The linear quadratic (LQ) model describes the fraction of surviving cells (S) after an irradiation dose (D) as follows: $S\,(D) = e^{\,-\alpha D - \beta D^2}$

In the LQ model, the linear component ($-\alpha D$) represents the lethal cell damage caused by a single radiation interaction resulting in a double-strand break. The quadratic component ($-\beta D^2$) represents the lethal cell damage caused by multiple radiation interactions, each resulting in single-strand breaks (sublethal damage) which are close enough together to cause double-strand breaks (lethal damage). The parameters α and β indicate the radiosensitivity of the irradiated cells. Rapidly

proliferating cells are more sensitive to radiation then tissue composed of cells with a slower cell turnover. Therefore, early responding tissue (including most malignant tumours) has a high α/β ratio, whereas late responding tissue (including brain tissue) has a low α/β ratio (9).

The cell survival curve is often referred to as a 'shouldered' dose-response curve, which has an initial linear component followed by an increasing curvature as the quadratic component becomes more important. The α/β ratio defines the curvature of the survival curve as it represents the dose level at which the linear and quadratic component have the same contribution (Fig. 6a). Thus, cells with a high α/β ratio have a relatively constant rate of cell killing with increasing dose, whereas cells with a low α/β ratio have an increasing rate of cell killing with increasing dose (Fig. 6b) (9).

Furthermore, the α/β ratio is a measure of the sparing effect of fractionation. Fractionation is a fundamental principle in RT (1). The total prescribed dose is divided into several small doses or fractions. These fractions are administered separately over time. This allows normal brain tissue (low α/β ratio) to recover from the sublethal damage of the initial radiation exposure. This tissue will respond to subsequent irradiation in line with the initial exposure. Tissue with a low α/β ratio, is more sensitive to the sparing effect of fractionation than tissue with a high α/β ratio (Fig. 6c). The aim of fractionation is maximising tumour (high α/β ratio) destruction and limiting damage to normal tissue (low α/β ratio) (9).

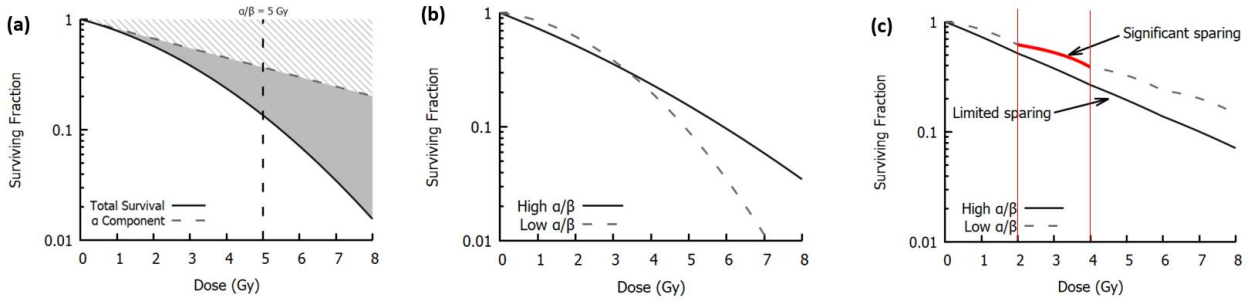

Fig. 6 Illustration of the linear quadratic model. Linear quadratic model separation into linear component (shaded area) and quadratic component (grey area) (a), linear quadratic model in early (high α/β) and late (low α/β) responding tissue (b), impact of fractionation (2 Gy fractions, vertical red lines) (c) adapted from (9).

1.3.4.2 Relative biological effectiveness

Relative biological effectiveness (RBE) is defined as the ratio of a dose of a reference radiation (photons) to the dose from another radiation modality to achieve the same biological effect. In proton treatment planning, the RBE is used to convert the physical proton dose into a biological effective dose. This dose is supposed to give an equivalent response as a photon treatment. This

conversion allows to apply the long-term clinical experience of photon treatments. In current clinical practice a fixed RBE value of 1.1 is used. This value is based on experimental data. An RBE value of 1.1 implies that for the same biological effect, 10% less irradiation dose is needed when using protons compared to photons. This is because protons have a higher ionization density than photons resulting in an increased efficiency of cell killing. However, clinical data suggest significant variations of RBE which are not considered in current treatment planning (6, 10).

1.3.4.3 Linear energy transfer

The linear energy transfer (LET) is the mean energy transferred per unit length by an ionizing particle due to electronic interactions. The more energy is transferred, the more ionization occurs. This implies that LET is a measure of ionisation density. High LET particles are more biologically effective than low LET particles. The main reason is the spatial distribution of the DNA damage within the tumour cells. Particles with high LET generate clustered damage which is more difficult to repair. For a proton beam, the LET value varies along the beam path. Therefore, it is beneficial to use averaged LET values such as the track or dose averaged LET (6). Track averaged LET (LET_t) is calculated by dividing the track into equal lengths and averaging the energy transferred in each length. Dose averaged LET (LET_d) is calculated by dividing the track into equal energy intervals and averaging the lengths of these intervals. Figure 7 demonstrates a visual representation of both values.

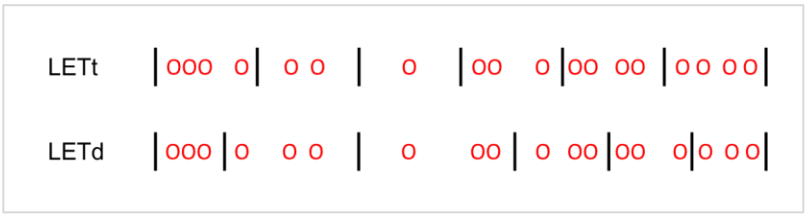

Fig. 7 Visual representation of LET_t and LET_d; red circles represent energy deposition; black lines represent a distance demarcation.
Abbreviations: LET_t, track averaged LET; LET_d, dose averaged LET

1.3.5 Reimbursement in Belgium

Not all paediatric CNS tumours can be treated with proton therapy. In the Belgian healthcare system, only patients who meet the stipulated conditions can receive reimbursement for their radiation therapy. For example, proton therapy is indicated for certain CNS tumours in patients less than 20 years old, provided the goal of treatment is to cure the patient. It is beyond the scope of

this master's thesis to describe all the reimbursement conditions. For an overview of these conditions, reference is made to the website of the RIZIV (11).

1.4 Aim of the study

Improvements in the management of CNS tumours have caused increased survival rates in children. This emphasizes the importance of the long-term safety and impact on quality of life of current treatment modalities (12). Theoretically, proton therapy should reduce treatment induced toxicity by limiting the irradiation dose to normal tissue and critical structures. However, unanticipated toxicities are reported in literature. Moreover, published data suggests a putative higher risk of imaging changes following proton therapy. The significance of these imaging changes is unknown. Therefore, further investigation of MRI changes after proton or photon radiotherapy for primary paediatric CNS tumours is required to understand the limitations and toxicity of these treatment modalities. The aim of this narrative review is to provide an overview and critical assessment of the published literature on MRI changes after proton or photon radiotherapy in paediatric brain tumours.

2 Methods

A narrative review was performed through database searching. We used keywords to define the population, intervention, comparison and outcome (PICO) of the research question. The purpose was to select a combination of search terms that covered each PICO element. The following electronic databases were used: PubMed and Embase. Table 1 gives an overview of the initial search terms used in each database. The literature research was last updated on 08/08/2022.

Table 1. PICO formatted search strategy

PICO	**Keywords**	**Search terms PubMed (MeSH)**	**Search terms Embase**
Population	Paediatric CNS tumours	Central nervous system neoplasms	Central nervous system tumor
Intervention	Proton therapy	Proton therapy	Proton therapy
Comparison	Photon therapy	Photons/therapeutic use	Photon therapy
Outcome	MRI imaging	Magnetic resonance imaging	Nuclear magnetic resonance imaging

Initially, no restrictions regarding the study population were applied since published literature of paediatric patients with CNS tumours is limited. Therefore, also literature discussing adult populations was assessed to get a comprehensive understanding of the subject. When processing the results, the articles without added value were excluded. Consequently, the age of the study population is not indicated as a valid exclusion criterion.

2.1 Pubmed

To identify appropriate search terms, the research question was entered in PubMed. MeSH terms assigned to given articles were evaluated. The MeSH hierarchy was used to identify related broader terms. Those best according to the meaning of the keywords were selected (Table 1).

The following search was performed: "Central Nervous System Neoplasms"[Majr] AND "Proton Therapy"[Majr] AND "Photons/therapeutic use"[Majr]. This resulted in 32 records. By using this combination, several articles were obtained in which both proton and photon therapy were applied simultaneously. These articles were excluded since this topic is not part of the research question. In addition, MRI changes were only discussed in a few articles. Based on these findings, we optimised the search. The term "Magnetic Resonance Imaging"[Majr] was added. This search was too specific as it resulted in 0 records. Therefore, all Majr topics except for "Central Nervous System Neoplasms" were changed to MeSH topics. This resulted in 6 records, the majority of which were

duplicates. To exclude the combination of proton and photon therapy, the logix AND was changed to OR which resulted in 8 records.

As these search strategies gave limited results, other terms were added such as “Brain neoplasms”. Furthermore, different subheadings such as “diagnostic imaging”, “radiotherapy” and “adverse events” were selected. However, this resulted in only 7 records. Therefore, the search strategy was widened and 36 reviews of the following search term were imported for screening: "Central Nervous System Neoplasms"[Majr] AND "Proton Therapy"[Majr].

By performing a citation-based search, related articles were obtained. To complete the search, references within selected articles were evaluated. Both methods resulted in 69 records. Taken together, 158 articles were imported for screening.

2.2 Embase

In Embase, only the PICO search was applied. Based on the records obtained in Pubmed, the terms "radiation necrosis" or "pseudoprogression” were added. The search strategies are shown in Table 2. In Embase, 14 records were imported for screening.

Table 2. PICO formatted search strategy

PICO	**Search 1**	**Search 2**	**Search 3**
Population	Central nervous system tumor/ exp	Central nervous system tumor/ exp	Central nervous system tumor/ exp
Intervention	Proton therapy/ exp	Proton therapy/ exp	Proton therapy/ exp
Comparison	Photon therapy/ exp	Photon therapy/ exp	Photon therapy/ exp
Outcome	Imaging changes/ all	Magnetic resonance imaging/ exp AND radiation necrosis/ exp	Pseudoprogression/ exp

2.3 Screening

In Pubmed and Embase, 172 records were imported for screening. Eight additional records were identified through other sources. From these 180 records, 16 duplicates were removed and 43 articles were excluded by title or abstract. Full-text articles were assessed for eligibility. A PRISMA flow diagram demonstrates the selection process and exclusion criteria (Fig. 8). Finally, 53 records were included in the review.

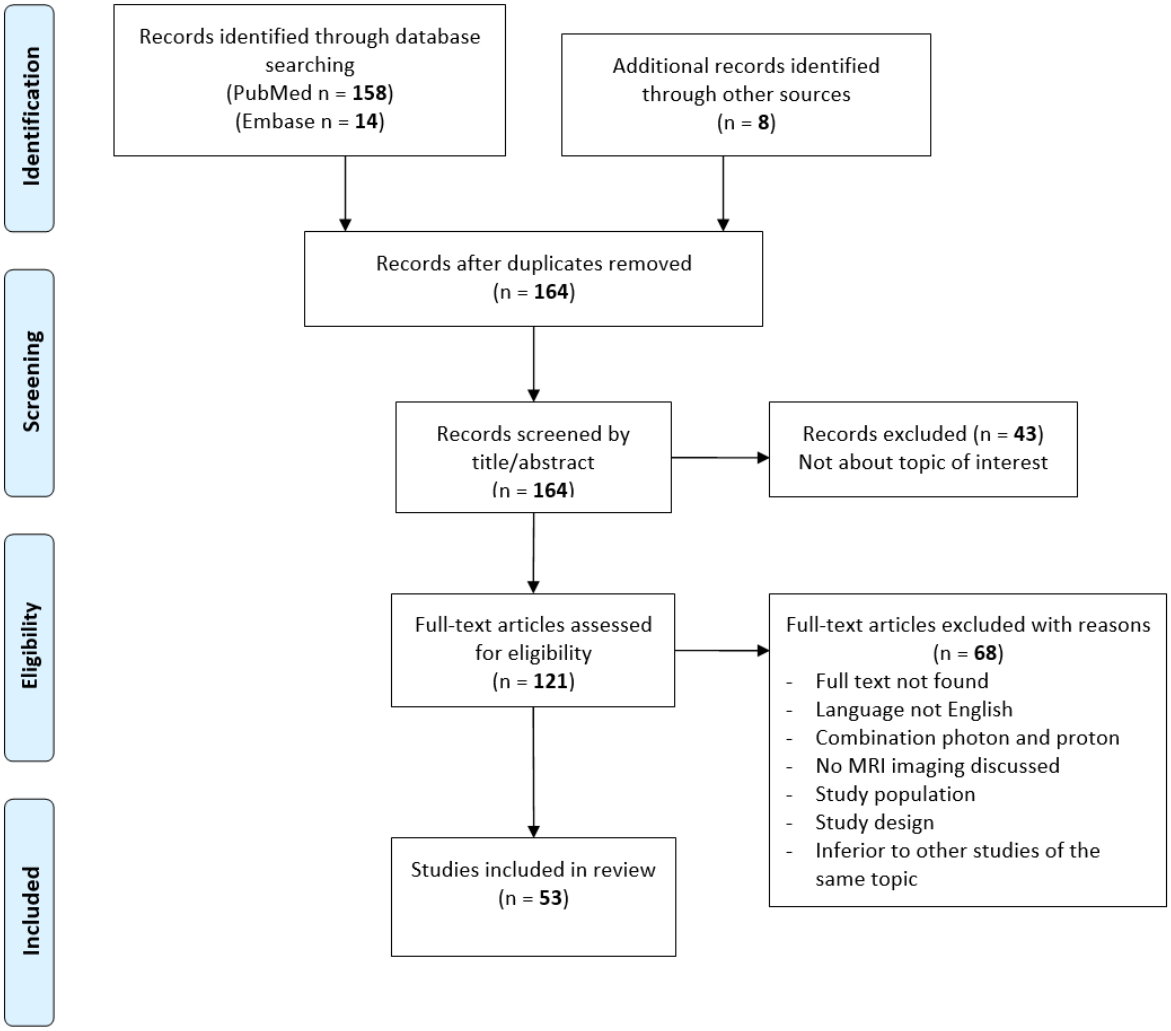

Fig. 8 PRISMA flow diagram.

3 Results

In our results, we mainly focus on original clinical studies. All patient characteristics and treatment details are summarized in Table 10, 11 and 12. Several studies describe imaging changes, the definitions and the details of which are shown in Table 13, 14 and 16.

To allow comparison between studies, we also looked for a standard validated grading scale for adverse events. The Common Terminology Criteria for Adverse Events (CTCAE) is such a severity grading scale for adverse events in oncological settings (13). The CTCAE version 4.0 for CNS necrosis is shown in Table 3. The descriptions of severity are based on a general guideline shown in Table S4 (supplementary data).

Table 3. CTCAE v4.0 CNS necrosis*

Grade	Criteria
1	Asymptomatic; clinical, or diagnostic observations only; intervention not indicated
2	Moderate symptoms; corticosteroids indicated
3	Severe symptoms; medical intervention indicated
4	Life-threatening consequences; urgent intervention indicated
5	Death

*CNS necrosis: a disorder characterized by a necrotic process occurring in the brain and/or spinal cord.

Abbreviations: CTCAE v4.0, Common Terminology Criteria for Adverse Events version 4.0; CNS, central nervous system. (13)

RT is an essential treatment modality in the management of paediatric CNS tumours. However, specific recommendations and guidelines on dose constraints in paediatric patients are lacking and are thus based on adult data. In 2018, the European Particle Therapy Network (EPTN) group formulated a consensus on dose constraints for OARs (14). These dose constraints relate to conventional photon and proton RT. The consensus is based on a comprehensive analysis of published literature. However, paediatric data was again not covered. An overview of the EPTN-consensus is shown in Table 4. Only OARs potentially relevant for this master's thesis are included. The EPTN group recommends the use of the EPTN-consensus to compare photon and proton RT. In current clinical practice, the Quantitative Analysis of Normal Tissue Effects in the Clinic (QUANTEC) guidelines are followed regarding brainstem dose constraints (15). This QUANTEC guideline recommends that 100% of the brainstem may receive 54 Gy and smaller volumes (1-10 cc) may receive up to 59 Gy (< 2 Gy per fraction) with a < 5% risk of severe brainstem toxicity.

Table 4. EPTN-consensus OAR dose constraints

OAR	α/β (Gy)	Dose constraint EQD2	Toxicity
Brain	2	$V_{60\ Gy} \leq 3$ cc	Symptomatic brain necrosis
Brainstem	2	Surface $D_{0.03\ cc} \leq 60$ Gy Interior $D_{0.03\ cc} \leq 54$ Gy	Permanent cranial neuropathy or necrosis
Chiasm and optic nerve	2	$D_{0.03\ cc} \leq 55$ Gy	Optic neuropathy
Hippocampus	2	$D_{40\%} \leq 7.3$ Gy	Memory loss
Pituitary	2	$D_{mean} \leq 45$ Gy $D_{mean} \leq 20$ Gy	Panhypopituitarism Growth hormone deficiency

Abbreviations: OAR, organ at risk; EQD2, equivalent dose in 2 Gy per fraction; V_{60}, volume receiving ≥ 60 Gy; $D_{0.03\ cc}$, near maximum dose to 0.3 cc of the structure/organ; D_{mean}, mean dose; $D_{40\%}$, mean dose to 40% of the volume of both hippocampi. (14)

Numerous intrinsic and extrinsic factors influence RT effects. Intrinsic factors include tumour location and anatomical changes during treatment, whereas extrinsic factors comprise surgery and chemotherapy. Fjæra et al. (16) focus their study on tumour location. They investigated how different paediatric posterior fossa tumour locations influence LET_d and biological dose to the brainstem during IMPT. Treatment plans were simulated for 4 tumour locations with a prescribed dose of 59.4 Gy. LET_d and biological dose (biological dose = physical dose (D) × RBE_{LET} with $RBE_{LET} = 1 + c \times LET_d$) were calculated. To make the RBE_{LET} represent variations in the biological effect due to LET, a scaling parameter *c* was applied. However, D × RBE_{LET} is only an approximation of the biological dose. In addition, the potential reduction in dose homogeneity was evaluated by comparing D × $RBE_{1.1}$ to D × RBE_{LET}. The observed brainstem and planning target volume (PTV) values of the simulated treatment plans are shown in Table 5.

Table 5. Values of simulated treatment plans

	Mean LET_d (range) [keV/µm]		Mean D × RBE_{LET} (range) [Gy (RBE)]		Mean D × $RBE_{1.1}$ (range) [Gy (RBE)]	
Plan	**Brainstem**	**PTV**	**Brainstem**	**PTV**	**Brainstem**	**PTV**
FO	3.2 (2.5–5.2)	3.0 (2.5–4.1)	54.0 (7.0–63.0)	60.4 (57.6–63.8)	52.9 (6.8–62.0)	59.7 (56.2–62.9)
HO	4.5 (2.8–8.9)	3.0 (2.5–4.3)	43.1 (0.9–62.6)	59.9 (55.7–63.4)	41.3 (0.8–61.3)	59.4 (53.2–62.7)
JP	5.9 (3.4–9.6)	3.0 (2.5–4.3)	15.7 (0.0–60.6)	60.5 (56.0–64.7)	14.4 (0.0–57.7)	59.8 (54.5–64.0)
JP_S3	5.9 (3.4–9.2)	3.0 (2.6–4.3)	15.8 (0.0–60.9)	60.4 (55.7–64.5)	14.5 (0.0–58.0)	59.8 (54.3–63.9)
JP_S9	5.9 (3.6–10.0)	3.0 (2.4–4.7)	16.7 (0.1–61.5)	60.5 (55.7–65.3)	15.3 (0.0–58.1)	59.8 (54.2–64.4)
1cmP	6.6 (4.3–14.9)	3.1 (2.4–4.3)	1.8 (0.0–35.5)	60.1 (56.0–64.2)	1.6 (0.0–33.0)	59.6 (54.8–63.5)

For the brainstem: highest values are indicated in red, lowest values are indicated in blue.

Abbreviations: FO, full overlap; HO, half overlap; JP, juxtaposed posterior; JP_S3, juxtaposed posterior spot size 3 mm; JP_S9, juxtaposed posterior spot size 9 mm; 1cmP, 1 cm posterior; LET_d, dose averaged LET; D, physical dose; RBE, relative biological effectiveness; PTV, planning target volume. (16)

The highest LET_d values occurred near the distal end of the treatment fields. Consequently, these high LET areas may overlap with the brainstem depending on the tumour location. For instance, the highest brainstem LET_d values were seen with the tumour located 1 cm posterior to the brainstem, whereas lower and more homogeneous LET_d values were seen when the tumour invaded the brainstem. In contrast, the highest brainstem $D \times RBE_{LET}$ values were seen when the tumour invaded the brainstem. Furthermore, the mean RBE_{LET} and $RBE_{1.1}$ values for the PTV were similar for all tumour locations. The differences between $D \times RBE_{LET}$ and $D \times RBE_{1.1}$ were mainly present at the distal edges of the PTV. A visual representation of these observations is shown in Figure 9. When increasing the spot distance (3 mm to 9 mm), there were no clear differences in the brainstem LET_d distributions. However, a slightly higher mean $D \times RBE_{LET}$ and $D \times RBE_{1.1}$ were observed for a larger spot distance.

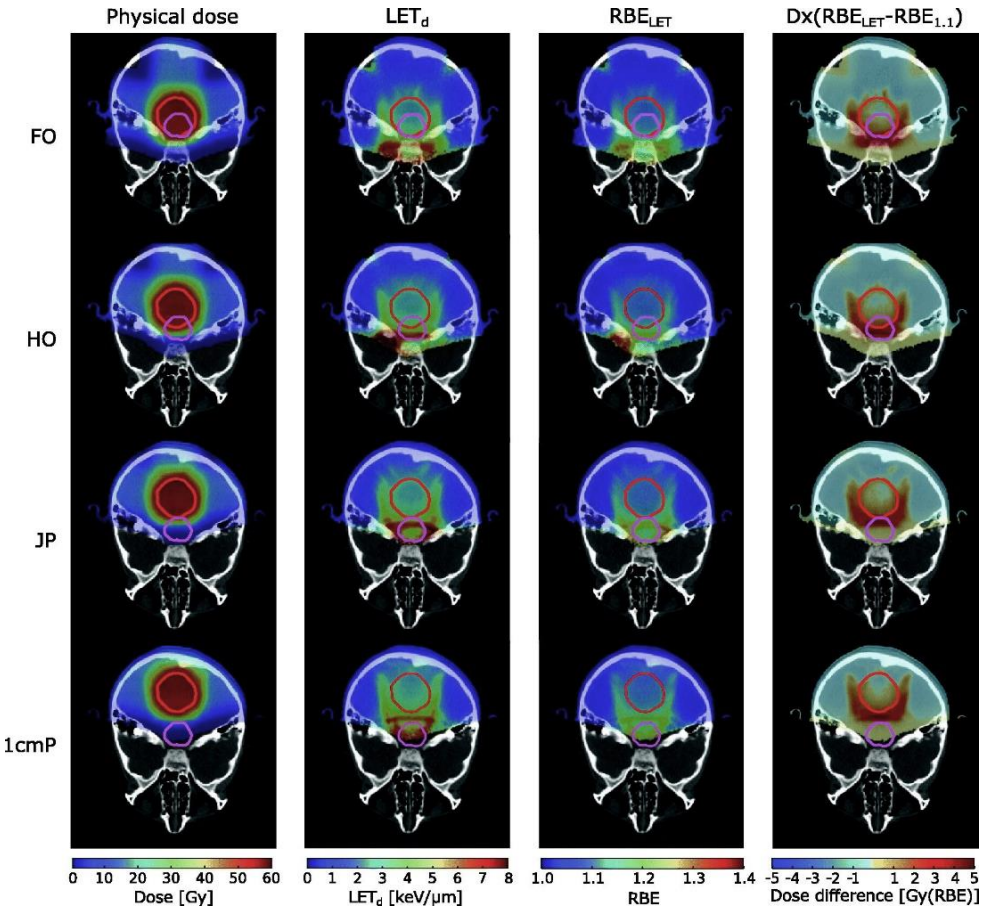

Fig. 9 Distributions of physical dose (column 1), LET_d (column 2), RBE_{LET} (column 3), and dose difference between $D \times RBE_{LET}$ and $D \times RBE_{1.1}$ (column 4) for treatment plans with different tumour locations. Positive values for the difference plots (column 5) indicate higher dose using RBE_{LET}. Different tumour locations relative to the brainstem: full overlap (FO); half overlap (HO); juxtaposed posterior (JP) and 1 cm posterior (1cmP). The PTVs are indicated in red and the brainstem in magenta. (16)

Anatomical changes during treatment are another intrinsic factor influencing RT effects. A case study (17) assessed the impact of these anatomical changes on photon and proton (IMPT) treatment plans. This was illustrated by recalculating a clinical case. In this case, the tumour was close to OARs with a postsurgical oedema along the beam path. For proton plans, an increase in oedema changed the dose distribution for all OARs. The D_{max} of the brainstem and optical nerve increased with 5.1 and 6.4 Gy(RBE), respectively. A reduction in oedema resulted in decreased target coverage. In contrast, photon plans remained nearly unchanged. The authors conclude that proton RT is less robust to anatomical changes than photon RT. This is due to the fixed radiological range of the proton beams.

Besides these intrinsic factors, also extrinsic factors such as surgery and chemotherapy may influence RT effects. Uh et al. (18) determined the effects of surgery and proton RT on white matter integrity in 51 paediatric craniopharyngioma patients. The FA of the corpus callosum was analysed. This white matter structure is often affected by surgery and receives a relatively high radiation dose in craniopharyngioma patients. In the corpus callosum, the surgery-affected regions showed a 20% lower FA compared to the unaffected regions ($p = .0001$). Moreover, 3 months after proton RT, both regions showed an FA reduction. This reduction was more significant in surgery-affected regions than in unaffected regions (9.2% vs. 1.3%, $p = .0083$). The authors conclude that surgical defects affect white matter integrity and appear to enhance the radiation dose effect.

In addition to surgery, also chemotherapy is one of the extrinsic factors, described in the study of Sabin et al. (19). The authors evaluated the combined effect of chemotherapy and proton RT in 17 paediatric patients. Eight patients developed MRI changes including T2 hyperintensity and T1 hypointensity after a median of 3.9 months. In 6 patients, these imaging changes were located within or adjacent to the high-dose volume. Four patients had mild and transient symptoms associated with their imaging changes. The imaging changes spontaneously decreased or resolved after a median of 2.3 months. These observations were compared to previous reports of patients treated with photon RT. The authors observed a similar appearance, but an earlier onset and regression for proton compared to photon related imaging changes. The authors suggest that the combined effects of treatment modalities and the sensitivity of the paediatric brain to therapy-induced damage should be considered as potential causes of the observed imaging changes.

Imaging changes are often observed during follow-up. However, the significance of these changes has not been sufficiently established. Therefore, Gunther et al. (20) performed a retrospective analysis of MRI changes in 72 paediatric ependymoma patients treated with postoperative RT (37 proton, 35 photon IMRT). Sixteen proton and 6 photon patients developed imaging changes. These

imaging changes occurred earlier after proton than after photon RT (median 3.8 vs. 5.3 months). The observed changes were mainly T2 hyperintensity and T1 enhancement. Haemorrhage and focal necrosis were only seen after proton RT. The authors identified risk factors for the development of imaging changes. Age ≤ 3 years and proton RT were associated with an increased risk of imaging changes (p =.05 and p =.019, respectively). In contrast, chemotherapy and a longer interval between surgery and RT trended towards a lower risk (p =.099 and p =.129, respectively). Furthermore, brainstem dose parameters were evaluated in the patients with infratentorial tumours treated with proton RT. In these patients, a D_{mean} ≥ 44.2 Gy(RBE) and $D_{50\%}$ ≥ 54 Gy(RBE) were associated with a higher risk of imaging changes (p =.016 and p =.024, respectively). Seven patients with imaging changes had symptoms requiring intervention. Three of these patients had persistent neurological disorders. One child died from complications of radiation necrosis (RN). The characteristics of this patient are shown in Table 15. There were no significant risk factors for the development of symptomatic imaging changes.

Another retrospective analysis of MRI changes was performed by Eichkorn et al. (21). They analysed 227 patients, including 42 children and 185 adults, treated with proton RT for low-grade glioma (LGG). During MRI follow-up, 49 patients developed radiation-induced contrast enhancement (RICE). These imaging changes were mainly observed within the second year after proton RT. The RICE rate in children was significantly lower than in adults (5% vs. 25%, p =.0043). In adults, the RICE rate was higher in older patients (p =.00128) and in patients diagnosed with WHO grade 2 vs. grade 1 tumours (24% vs. 8%, p =.026). The association between WHO grading and RICE was independent of age (p =.04) and radiation dose (p =.005) but not independent of IDH mutational status (p =.11). Out of 49 patients with RICE, 26 were symptomatic. According to the CTCAE v4.0, grade 0, 1, 2 and 3 toxicity occurred in 23, 12, 0 and 14 patients, respectively. Moreover, overall survival was not affected by RICE. The authors conclude that RICE depends on tumour characteristics and patient's age. WHO grade 2 and older age were identified as independent factors associated with subsequent development of RICE. According to the authors, RICE is more rare in children than in adults after proton RT for LGG.

Harrabi et al. (22) reviewed the incidence of RICE following proton RT in 110 LGG patients. During MRI follow-up, 31 patients developed 1 or more RICE lesions (number of lesions n = 51). From each voxel receiving > 40 Gy, LET_d and the distance to the ventricles were determined. Of all RICE lesions, 26 lesions were located in a high LET_d area (≥ 5.0 keV/µm) at the distal end of the proton beam and 32 lesions were close to the ventricles (≤ 4mm). The authors conclude that high LET_d (p =.003) and periventricular location (p <.001) are predictive factors for the development of RICE. In the same population, Bahn et al. (23) focused on the RICE lesions outside the tumour

volume, in contrast to previous authors (22) who analysed RICE lesions both inside and outside the tumour volume. The authors developed a model that predicts the risk and location of possible radiation-induced lesions. Their findings provide clinical evidence for an increased periventricular radiation sensitivity and an RBE that increases significantly with increasing LET_d (e.g. RBE 1.2 for LET_d = 2 keV/µm and RBE 1.5 for LET_d = 5 keV/µm).

There is growing evidence that the RBE varies along the SOBP (24). However, there is little knowledge about the clinical relevance of these variations. Therefore, Peeler et al. (25) investigated whether areas of normal tissue damage are associated with increased biological dose effectiveness. Among 34 paediatric patients with ependymoma, 14 patients developed imaging changes after proton RT. Treatment plans of these patients were recalculated to obtain LET and dose distributions. Areas with imaging changes had increased LET values. Moreover, the physical dose at which imaging changes occurred was lower when combined with elevated LET values. This indicates an increase in biological dose effectiveness with increased LET. Furthermore, maximum LET_t > 2.5 keV/µm was significantly associated with the presence of imaging changes (p =.02). This study confirms that imaging changes are associated with both physical dose and LET. Moreover, it provides clinical evidence of a variable proton biological effectiveness. The authors made a generalized linear model to estimate the risk of imaging changes based on physical dose and LET_t. This model can be used to optimise a treatment plan and reduce the risk of normal tissue damage. A visual representation of this model is shown in Figure 10. The authors suggest that analysing additional clinical data may allow to develop different models (e.g. for different ages).

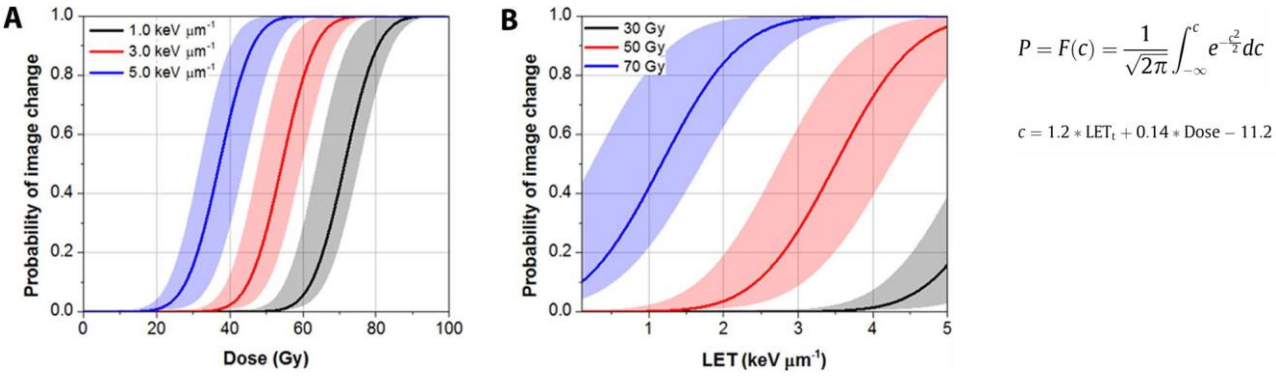

Fig. 10 Representations of the generalized linear model for predicting imaging change from constant LET_t or physical dose. Curves represent (A) constant LET_t of 1, 3, and 5 keV/µm and (B) constant physical dose of 30, 50, and 70 Gy. Shaded bands indicate 95% confidence intervals. (25)

Besides general MRI changes, some studies focus on specific imaging changes such as RN or pseudoprogression (PsP). A case series (26) presented 2 paediatric patients treated with postsurgical proton RT. Early after treatment, both patients developed imaging changes within or near the radiation field. These imaging changes were consistent with RN**.** During follow-up, both patients remained asymptomatic and achieved complete radiographic resolution. Details of the case series are shown in Table 6.

Table 6. Case series

Case	Age (years)	Histology	Surgery	RT modality	Median RT dose (Gy (RBE))
1	14	Anaplastic ependymoma	GTR	Proton	50.4
2	9	Medulloblastoma	GTR	Proton	54.0

Abbreviations: RT, radiotherapy; RBE, relative biological effectiveness; GTR; gross total resection. (26)

Furthermore, Kralik et al. (27) focused their study on the development of RN after proton RT. Among 52 paediatric patients, 16 patients (31%) demonstrated radiographic signs of RN. The median time to the development and resolution of RN was 5 and 5.3 months, respectively. According to the CTCAE v4.0, 4 patients had grade 3 toxicity. AT/RT histology and the combination of multiple (> 3) chemotherapeutic agents were identified as risk factors for developing RN (p =.03 and p =.03, respectively). However, it was not possible to determine the impact of specific chemotherapeutic agents. Ependymoma histology, young age, surgery and total radiation dose were not statistically significantly associated with the development of RN.

In another study (28) of 171 paediatric patients treated with proton RT, 29 patients (17%) developed RN at a median of 5 months. According to the CTCAE v4.0, grade 1, 2, 4 and 5 toxicity occurred in 17, 8, 2 and 2 patients, respectively. The characteristics of the 2 patients with grade 5 toxicity are shown in Table 15. Both patients had RN of the brainstem. They were < 3 years old and were treated for infratentorial tumours. Ependymoma histology, chemotherapy and hydrocephalus before proton RT were significant predictive factors for RN (p =.026, p =.003 and p =.035, respectively). In addition to RN, white matter lesions were observed in 18 patients (11%) at a median of 14.5 months. For these lesions, grade 1, 2 and 3 toxicity occurred in 13, 4 and 3 patients, respectively.

White matter lesions were also investigated by Fouladi et al. (29). MRI scans of 127 paediatric patients with medulloblastoma or PNET were evaluated. All patients received RT followed by high-dose chemotherapy with stem cell rescue. The authors reported 22 patients (17%) with white matter lesions. Most of these lesions occurred in the posterior fossa, including 10 lesions

in the brainstem. White matter lesions were graded by appearance on MRI (Table 7). According to this classification, grade 1 and 2 occurred in 7 and 15 patients, respectively. Only 3 patients developed symptoms. Two of these patients had brainstem lesions and one patient had periventricular imaging changes. No significant predictive factors were found for the development of the observed white matter lesions.

Table 7. Classification of white matter lesions

Grade	Criteria
1	Abnormal signal intensity on T2
2	Increased signal intensity on T2 and contrast enhancement on T1
3	Evidence of haemorrhage
4	Encephalomalacia or focal necrosis

Harreld et al. (30) calculated the supratentorial white matter magnetization transfer ratio (MTR) of 95 paediatric medulloblastoma patients before treatment. The MTR is a measure of myelin density. After treatment, 23 patients developed RN. In these children, the mean MTR was significantly lower ($p = .03$) compared to those without RN. The authors conclude that decreased myelin density may be a predictive factor for RN and may indicate children at risk.

All previous studies describe RN after proton RT. In contrast, Plimpton et al. (31) investigated RN after photon RT. In a study of 101 children treated with photon RT, 5 patients (5%) developed imaging changes consistent with RN at a median of 1.2 months. All these patients had glial tumours (2 HGG, 3 LGG) and received an average dose of 56.2 Gy. Three patients had symptoms associated with their imaging changes. Age, radiation dose and chemotherapy were not associated with the development of RN.

In addition to RN, also PsP is one of the observed imaging changes after RT. Ritterbusch et al. (32) compared PsP imaging patterns of patients receiving proton RT with those receiving photon RT. The authors observed differences in the appearance, area and timing of PsP. Proton PsP appeared to be small (< 1cm), multifocal and oval to round, whereas photon PsP was less nodular. Regarding the area, photon PsP was directly associated with the resection cavity, whereas proton PsP occurred about 2 cm from the resection cavity at the distal end of the proton beam. Moreover, since proton PsP developed later than photon PsP (15.4 months vs. 3 months), proton PsP would be incorrectly considered as tumour progression according to current guidelines. From these findings, the authors conclude that proton and photon RT result in different imaging changes.

Furthermore, overall survival was not affected by the presence of proton PsP (p =.57) whereas nothing was mentioned about photon PsP.

Another study (33) evaluated PsP on follow-up MRI scans of 136 children with LGG treated with first-line RT (25 proton, 60 photon, 51 brachytherapy). “Suspected” and “definite” PsP were distinguished based on 4 radiological criteria shown in Table 8. The pattern of these criteria suspected PsP in 71 patients (52%) while definite PsP was diagnosed in 54 patients (40%). After proton, photon or brachytherapy, PsP occurred at a median of 6.5, 4.4 and 7.2 months, respectively. The onset of definite PsP depended on the used radiation modality (p =.028), with PsP after brachytherapy starting significantly later than PsP after photon RT (p =.012). When comparing the 3 radiation modalities, there were no differences in PsP rates, duration and appearance. Furthermore, tumour histology or radiation dose were not associated with the development of PsP. Overall and progression-free survival did not differ between patients with and those without PsP. The authors conclude that increased contrast enhancement and perifocal tumour oedema are indications of the presence of PsP. Moreover, intratumoural necrosis proved to be a relevant predictor of definite PsP (p < .001).

Table 8. Radiological criteria for PsP

Criteria	Suspected PsP		Definite PsP
CE fraction	↑	⇨	↘
CE intensity	↑	⇨	↘
Focal tumour associated T2 lesion	↑	⇨	↘
Total tumour associated T2 lesion	> 25% ↑	⇨	↘ or stable

Abbreviations: PsP, pseudoprogression; CE, contrast enhancement; ↑, increase; ↘, regression; ⇨, evolution during follow-up. (33)

Ludmir et al. (34) investigated the incidence of PsP in 83 paediatric LGG patients treated with proton or photon RT. PsP was more common in patients treated with proton RT and in patients treated with a higher radiation dose (>50.4 Gy(RBE)). Multivariate analysis confirmed radiation modality (p =.025) and radiation dose (p =.005) as significant and independent predictors of PsP. In contrast, age, tumour location and chemotherapy did not affect the PsP incidence. The authors suggest that high-dose areas may contribute to vascular lesions leading to PsP. Out of 31 patients with PsP, 6 were symptomatic. Moreover, 3 of these symptomatic patients, all treated with proton RT, required surgical intervention.

Besides RN and PsP, other radiation-induced imaging changes are observed during MRI follow-up. These imaging changes include damage to medium and large vessels. For instance, Hall et al. (35) investigated the incidence and severity of vasculopathy after proton RT. Among 644 paediatric patients, the 3-year cumulative incidence of any vasculopathy and serious vasculopathy was 6.4% and 2.6%, respectively. Most patients with vasculopathy were asymptomatic, whereas 29% of them presented with TIA or CVA. Age < 5 years and chiasm D_{max} ≥ 54 Gy were significantly associated with the development of any vasculopathy event (p=.002 and p <.001, respectively). Chiasm D_{max} ≥ 54 Gy was also a predictive factor for serious vasculopathy (p =.041). The authors suggest that the rate of vasculopathy after proton and photon RT is comparable.

The dosimetric and LET_d correlation in radiation-induced vasculopathy was analysed in another study (36). In this study, 2 of the 16 paediatric craniopharyngioma patients presented with vasculopathy. LET_d values in the vasculature structures were significantly higher in patients with vasculopathy (p =.02). Moreover, in these patients, high LET_d values were combined with high mean dose values. However, there was no correlation between dose distributions in the vascular structures and vasculopathy (p =.88).

In addition to medium and large vessel damage, microvascular complications can also cause imaging changes. Kralik et al. (37) investigated radiation-induced cerebral microbleeds (CMB) in 100 paediatric patients treated with proton RT. Approximately 80% of patients developed CMB. These lesions mainly appeared in the first 3 years after RT. No lesion showed resolution during follow-up. Younger age, higher D_{max} and a higher percentage and volume of the brain exposed to ≥ 30 Gy were significantly associated with the development of CMB (p =.0004, p =.001, p =.0004 and p =.0005, respectively). In contrast, chemotherapy was not identified as a significant risk factor (p =.35).

Of all these imaging changes, those in the brainstem are of particular concern. In a recent study (38), the authors analysed the incidence of brainstem injury in 468 paediatric patients treated with proton RT from 2007 to 2019. All patients received a brainstem D_{mean} > 30 Gy(RBE) and/or $D_{max\ 0.03\ cc}$ > 50.4 Gy. According to the CTCAE v4.0, grade 1, 2, 3, 4 and 5 toxicity occurred in 51, 7, 5, 1 and 2 patient(s), respectively. The characteristics of the 2 patients with grade 5 toxicity are shown in Table 15. Both patients were < 3 years old and were treated for infratentorial tumours. Since 2014, strict brainstem dose constraints of D_{mean} ≤ 52.4 Gy, D_{max} ≤ 57 Gy, and V_{54} ≤ 10% were applied. By applying these dose constraints, there was a trend towards a lower incidence of symptomatic brainstem injury compared to the period before this adaptation (1.5% vs. 4.4% p =.089). However, the incidence of asymptomatic radiographic changes remained similar. Age ≤ 3

years, female gender, AT/RT histology, high-dose chemotherapy with stem cell rescue before RT and not receiving craniospinal irradiation were significant predictive factors for symptomatic brainstem injury (p =.005, p =.004, p =.008, p =.001 and p =.016, respectively). Furthermore, patients with symptomatic brainstem injury had significantly higher $V_{50\text{-}52}$.

The previous study describes asymptomatic as well as symptomatic brainstem injury. Whereas the following studies only focus on the latter. Gentile et al. (39) reported 5 patients with symptomatic brainstem injury among 216 paediatric patients. All patients were treated with proton RT for posterior fossa tumours. According to the CTCAE v4.0, grade 2, 3 and 4 toxicity occurred in 1, 3 and 1 patient(s), respectively. High-dose chemotherapy with stem cell rescue and neurological complications after surgery were associated with an increased risk of brainstem injury (p =.04 and p =.02, respectively). The authors suggest that when $D_{max} < 55.8$ Gy and $V_{55} \leq 6.0\%$ the occurrence of symptomatic brainstem injury would be < 2%.

Indelicato et al. (40) reviewed 313 paediatric patients treated with proton RT. All patients received > 50.4 Gy to the brainstem. Overall, 11 patients developed symptomatic brainstem injury. According to the CTCAE v4.0, grade 2, 3, 4 and 5 toxicity occurred in 7, 1, 2 and 1 patient(s), respectively. The characteristics of the patient with grade 5 toxicity are shown in Table 15. Age < 5 years, posterior fossa tumour location and specific dosimetric parameters were associated with an increased risk of brainstem toxicity (p =.01, p <<.001 and p <.01, respectively). Several dosimetric parameters were defined, including brainstem $D_{max} > 56.6$ Gy, $D_{50\%} > 52.4$ Gy and $V_{55} > 17.7\%$. Among the patients who received $D_{50\%} \geq 52.4$ Gy, the toxicity rate was 10.5%. Furthermore, patients receiving GTR trended towards a higher toxicity rate (7.3% vs. 1.5%, p >.1). The authors suggest more conservative dosimetric guidelines for young patients with posterior fossa tumours, particularly those undergoing aggressive surgery.

A recent case-control study (41) investigated whether symptomatic brainstem toxicity is associated with a variable LET_d and RBE. Nine paediatric brain tumour patients treated with proton RT were each matched to three controls. Cases and controls were matched based on age (±1.5 years), diagnosis (craniopharyngioma or ependymoma), adjuvant treatment and brainstem dose characteristics. Variable RBE-weighted doses were calculated with two different RBE models. Since the biological effect depends on both LET_d and dose, multiple dose cutoffs were used to evaluate the isolated effect of LET_d. As a result, only voxels receiving doses above the applied cutoff were included in the calculations. Brainstem structures receiving doses above 54 Gy showed a 13% higher median LET_d (p =.08) and only a 2% higher median variable RBE-weighted dose (p =.6) for cases compared to controls. The authors conclude that increased LET_d could be a minor contributor to the observed brainstem toxicity.

A similar LET_d evaluation was performed by Giantsoudi et al. (42). The authors investigated the incidence of CNS injury in 111 paediatric patients treated with proton RT for medulloblastoma. All patients received CSI followed by an involved field or posterior fossa boost. Overall, 10 patients developed radiographic changes. According to the CTCAE v4.0, grade 1, 2, 3 and 4 toxicity occurred in 6, 1, 2 and 1 patient(s), respectively. Only patients with grade ≥ 2 were included in the definition of CNS injury. The characteristics of these patients are shown in table 9. Although the 6 asymptomatic patients had a brainstem D_{50} > 52.4 Gy, their radiographic changes were not located in the brainstem. The authors observed a trend towards a higher risk of CNS injury after a posterior fossa boost compared to an involved field boost (p =.094). Furthermore, LET values were compared between areas with radiographic changes and the entire boost target volume. Although 8 of these 10 areas had higher LET values than the target volume, no clear correlation was found between sites of toxicity and elevated RBE due to higher LET values (p =.12).

Table 9. Characteristics of patients with CNS injury

Patient	Age (year)	CSI dose (Gy(RBE))	PF or IF boost (dose in Gy)	Brainstem D_{max} (Gy(RBE))	Brainstem D_{50} (Gy(RBE))	Location of MRI changes	Grade
1	8.2	23.4	PF (30.6)	56.17	55.0	Brainstem	3
2	6.4	23.4	IF (30.6)	55.00	50.17	Brainstem	3
3	23.0	23.4	PF (30.6)	55.85	54.55	Brainstem	4
4	13.4	23.4	PF (30.6)	56.02	54.56	Upper cervical cord	2

*These patients had notable sensitivities to chemotherapeutic agents.

Abbreviations: CSI, craniospinal irradiation; PF, posterior fossa; IF, involved field; $D_{max,}$ maximum dose; D_{50}, mean dose to 50% of the irradiated volume; RBE, relative biological effectiveness. (42)

All previous studies describe brainstem injury after proton RT. In contrast Devine et al. (43) investigated brainstem injury after photon RT. All patients were treated for posterior fossa tumours with a median prescribed dose of 55.8 Gy, a median brainstem $D_{50\%}$ of 54.9 Gy and a median V_{55} of 85%. These dosimetric parameters were selected based on the study of Indelicato et al. (40), in which they were correlated with a brainstem toxicity rate of 10.5% after proton RT. Among 107 paediatric patients, 2 patients developed grade 1 brainstem RN. Based on these observations, the authors suggest a minimal risk of brainstem toxicity after photon RT.

Hua et al. (44) analysed the evolution of brainstem FA and ADC in 20 paediatric patients after photon RT. In all patients, the brainstem was located in the radiation field. However, the brainstem dose did not exceed the tolerance threshold of 54 Gy. Three patterns were observed in the FA evolution: (1) a normal or stable developing trend; (2) an initial decline with subsequent recovery; and (3) a progressive decline without evidence of complete recovery. Figure 11 provides

a visual representation of these patterns. Although generally opposite to FA patterns, ADC patterns were less distinctive. Patients with incomplete recovery often had a larger decline in FA within the first year after RT. The authors conclude that an early response in brainstem FA could be used as an indicator of the recovery trend over 5 years after RT. The authors hypothesize that the variable white matter response is a combined effect of radiation dose, clinical risk factors and individual ability to repair therapeutic damage.

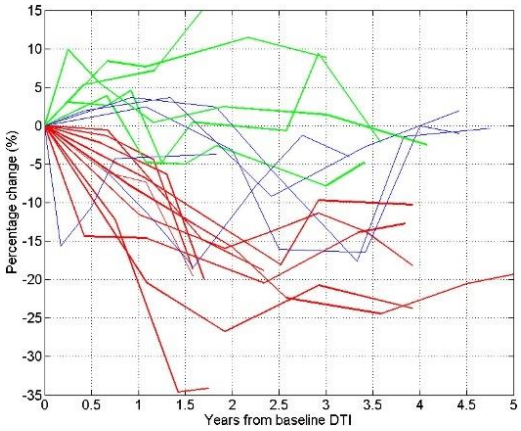

Fig. 11 The longitudinal percentage change from baseline FA of the pons for 20 patients. Each line represents a patient, each collar represents an FA pattern: (green) normal or stable; (blue) initial decline with subsequent recovery; (red) progressive decline. (44)

Finally, Roberts et al. (45) analysed the spatial correlation of imaging changes with a novel biologic dose model. Among 30 patients, 7 patients developed imaging changes after proton RT (spot scanning). The observed T2/FLAIR changes were contoured. The volumetric overlap of these imaging changes with the treatment planning dose and the biologic dose was analysed. The biologic dose[1] demonstrated a superior spatial correlation with T2/FLAIR changes. According to the authors, using a biologic dose model in treatment planning may better predict hot spots in critical structures. Furthermore, receiving ≥ 56.6 Gy to the brainstem was associated with a significantly higher probability of radiation-induced imaging changes (p =.033), whereas only a higher trend could be observed for concurrent chemotherapy (vincristine) (p =.068).

Overall, 3 studies (16, 35, 40) reported the use of precautions to minimise the risk of theoretical RBE uncertainty at the end of the proton beam. This includes multiple field plans and permitting no more than 1/3 of the beams to end in brainstem tissue beyond the PTV.

[1] Biological dose was calculated from the physical dose and LET_d assuming a linear relationship: $BD = 1.1*TD\ (0.88 + 0.08*LET_d)$

Table 10. Patient characteristics and treatment details

Author[reference]	Year	Patients	Age (range) [years]	Gender ♀ - ♂	Histology (patients)	RT modality	Median RT dose (range) [Gy (RBE)]	Treatment before RT	Treatment after RT
Fouladi et al.[29]	2004	134	ND	ND	Medulloblastoma PNET	ND	Standard risk 23.4 to 55.8 (CSI + boost) High risk 36 to 55.8 (CSI + focal boost)	Surgery	Chemotherapy
Hua et al.[44]	2012	20	Median 7.0 (4.0-23.0)	8 - 12	HGG (10)	Photon	54-59.4	Erlotinib	Erlotinib
					Medulloblastoma (7) AT/RT (1) PNET (2)		55.8	Surgery	Chemotherapy
Sabin et al.[19]	2013	18	Median 1.8	ND	Ependymoma Medulloblastoma AT/RT PNET Choroid plexus ca.	Proton	54	Surgery Chemotherapy	Chemotherapy
Indelicato et al.[40]	2014	313	Median 5.9 (0.5-17.9)	145 - 168	LGG (66) Ependymoma (73) Medulloblastoma (38) Craniopharyngioma (68) Other (68)	Proton (PS)	54 (48.6-75.6)	Surgery (98%) Chemotherapy (50%)	
Gunther et al.[20]	2015	72	Proton median 2.8 (1.6-16.6) Photon median 6.1 (1.2-19.0)	31 - 41	Ependymoma	37 proton 35 photon (IMRT)	Proton 54 (50.4-59.4) Photon 59.4 (53.0-59.4)	Surgery (100%) Chemotherapy (5 proton, 7 photon)	Chemotherapy (5 proton)
Uh et al. [18]	2015	51	Median 9.2 (2.1-19.3)	29 - 22	Craniopharyngioma	Proton (PS)	54	Surgery	NA
Kralik et al.[27]	2015	52	Mean 7.2 (0.8-18)	15 - 37	Glioma of the brainstem (3) Ependymoma (12) Medulloblastoma/PNET (19) AT/RT (3) Craniopharyngioma (3) Other (8)	Proton	54 (21-59.4)	Surgery (98%) Chemotherapy (26%)	Chemotherapy (54%)
Plimpton et al.[31]	2015	101	Mean 9.3 (1.0-21.8)	ND	HGG (15) LGG (12) Ependymoma (18) Medulloblastoma/PNET (30) AT/RT (3) Craniopharyngioma (9) Other (14)	Photon	54 (30-60)	Chemotherapy (73%)	ND
Giantsoudi et al.[42]	2016	111	Median 7 (2.7-22)	45 - 66	Medulloblastoma	Proton (PS)	54.0 (50.4-59.4) CSI 23.4 (18-36) Boost 54.0 IF, 30.6 PF (62% IF, 38%PF)	ND	ND
Peeler et al.[25]	2016	34	Median 2.9 (1.3-19.0)	13 - 21	Ependymoma	Proton (PS)	57.6 (54.0-59.4)	Surgery (100%)	NA
Gentile et al.[39]	2018	216	Median 6.6 (0.5-23.1)	90 - 126	Ependymoma (56) Medulloblastoma (154) AT/RT (6)	Proton (PS)	54 (46.8-59.4) CSI 23.4 (18-39.6) Boost (78% IF, 22% PF)	Surgery (99%) Chemotherapy (83.3%)	NA
Hall et al.[35]	2018	644	Median 7.6 (0.7-21.8)	289 - 355	LGG (131) Ependymoma (135) Medulloblastoma (80) Craniopharyngioma (135) Other (163)	Proton (PS)	54 (25.2-75.6)	Surgery (95%) Chemotherapy (33%)	NA
Kralik et al.[37]	2018	100	Median 8.1 (0.75-18)	37 - 63	Ependymoma (19) Medulloblastoma (28) AT/RT (3) Craniopharyngioma (17) Other (33)	Proton	54 (30-59.4)	Surgery Chemotherapy	NA

Table 10. Patient characteristics and treatment details *(continued)*

Author[reference]	Year	Patients	Age (range) [years]	Gender ♀ - ♂	Histology (patients)	RT modality	Median RT dose (range) [Gy (RBE)]	Treatment before RT	Treatment after RT
Bojaxhiu et al.[28]	2018	171	Median 3.3 (0.3-17.0)	70 - 101	LGG (20) Ependymoma (64) Medulloblastoma (9) AT/RT (12) PNET (4) Germ cell tumour (8) Craniopharyngioma (15) Meningioma (4) Choroid plexus ca. (4) Chordoma (16) Chondrosarcoma (6) Other (9)	Proton (PBS)	54 (40.0-74.1)	Surgery (88%) Chemotherapy (61%)	Chemotherapy (19%)
Robertsen et al.[45]	2019	30	Median 11 (1.67-18)	12 - 18	Astrocytoma (5) Ependymoma (4) Medulloblastoma (10) Craniopharyngioma (2) Other (9)	Proton (spot PBS)	54 (50.4-59.4)	Surgery (80%) Chemotherapy	ND
Devine et al.[43]	2019	107	Median 8.3 (0.8-20.7)	45 - 62	LGG (1) HGG (12) Ependymoma (17) Medulloblastoma (66) AT/RT (6) PNET (3) Other (2)	Photon	55.8 (50.4-60.0) CSI 23.4 (18.0-39.6) (64%) Boost 24.4 (5.4-36.0) (80%)	Surgery (92%) Chemotherapy (37%)	NA
Ludmir et al.[34]	2019	83	Median 10 (1.0-17.6)	37 - 46	LGG	51 proton (96% PS, 4% PBS) 32 photon	Proton 50.4 (45-54) Photon 50.4 (45-59.4)	Surgery (22 proton, 19 photon) Chemotherapy (23 proton, 9 photon)	NA
Bolsi et al.[36]	2020	16	Median 9.5 (2.0-18.2)	10 - 6	Craniopharyngioma	Proton (PBS) (19% IMPT, 81% SFUD) (19% asymmetric, 81% symmetric)	54		
Harrabi et al.[22] Bahn et al.[23]	2020	110	Median 35 (2-63)	49 - 61	LGG	Proton (PBS)	54 (50.4-60)	Surgery (57%) Chemotherapy (35%)	NA
Ritterbush et al.[32]	2021	100	Proton mean 46.7 Photon mean 47.7	45 - 55	LGG	57 proton (PBS) 43 photon	ND	Surgery Chemotherapy	NA
Harreld et al.[30]	2022	95	Mean 11	39 - 56	Medulloblastoma	CSI: 42 proton, 53 photon Focal: 71 proton, 24 photon	Low risk 15 to 51 (CSI + focal boost) High risk 36 to 54 (CSI + focal boost)	Surgery	Chemotherapy
Eichkorn et al.[21]	2022	227	Median 36.5 (2.0-76.3)	99 - 128	LGG	Proton (raster PBS)	54 (50.0-60)	Surgery	Chemotherapy
*Eichkorn et al.[21]	2022	42	Median 12.8 (2.0-20.4)	20 - 22	LGG	Proton (raster PBS)	54 (50.0-60)	Surgery (56%)	Chemotherapy (26%)
**Eichkorn et al.[21]	2022	185	Median 40.0 (21.0-76.3)	79 - 106	LGG	Proton (raster PBS)	54 (50.4-57.6)	Surgery (75%)	Chemotherapy (75%)
Upadhyay et al.[38]	2022	468	Median 6.3 (0.2-18.6)	205 - 263	Glioma (114) Ependymoma (87) Medulloblastoma (200) AT/RT (43)	Proton (80% PS, 20% PBS ± PS)	54 (39.6-59.4)	Surgery (97%) Chemotherapy (46%)	

*Paediatric subpopulation

**Adult subpopulation

Abbreviations: ND, not defined; NA, not applicable; ♀, female; ♂,male; RT, radiotherapy; PS, passive scattering; PBS, pencil beam scanning; RBE, relative biological effectiveness; HGG, high-grade glioma; LGG, low-grade glioma; AT/RT, atypical teratoid/rhabdoid tumour; PNET, primitive neuroectodermal tumour; ca., carcinoma

Table 11. Chemotherapy agents

Author[reference]	Year	Chemotherapy before RT	Chemotherapy during RT	Chemotherapy after RT	Time not specified
Fouladi et al.[29]	2004	NA	NA	Cisplatin - cyclophosphamide - vincristine* (High dose chemotherapy 6 weeks after RT + stem cell rescue)	NA
Hua et al.[44]	2012	NA	NA	Cisplatin - cyclophosphamide - vincristine	NA
Sabin et al.[19]	2013	Cisplatin - cyclophosphamide - vincristine Methotrexate	NA	Cyclophosphamide - topotecan - erlotinib (medulloblastoma and ependymoma) Cyclophosphamide - topotecan - etoposide (other diagnoses)	NA
Indelicato et al.[40]	2014	ND	NA	NA	NA
Gunther et al.[20]	2015	ND	NA	ND	NA
Kralik et al.[27]**	2015	Total 14 patients Cisplatin - cyclophosphamide - etoposide - methotrexate - temozolomide (3) Cisplatin - cyclophosphamide - etoposide - methotrexate - vincristine (2) Carboplatin - cyclophosphamide - etoposide - vincristine (3) Carboplatin - etoposide (6)	Total 18 patients Vincristine (16) Carboplatin (2)	Total 29 patients Cisplatin - cyclophosphamide - vincristine (7) Cisplatin - cyclophosphamide - vincristine - lomustine (9) Cisplatin - cyclophosphamide - vincristine - etoposide (2) Cisplatin - cyclophosphamide - vincristine - etoposide - sunitinib(1) Cisplatin - cyclophosphamide - vincristine - topotecan - irinotecan bevacizumab (1) Cisplatin - vincristine - lomustine (1) Carboplatin - cyclophosphamide - thiotepa - topotecan (1) Carboplatin - tiotepa (4) Vincristine - lomustine - procarbazine - thioguanine (1) Temozolomide (1) Bevacizumab (1)	NA
Plimpton et al.[31]	2015	ND	ND	ND	ND
Gentile et al.[39]	2018	ND (74.1%)	ND (57.9%)	NA	NA
Hall et al.[35]	2018	ND (33%)	ND (17%)	NA	NA
Kralik et al.[37]	2018	ND	NA	NA	NA
Bojaxhiu et al.[28]	2018	ND (61%)	ND (18%)	ND (19%)	NA
Devine et al.[43]	2019	ND (37%)	ND (57.9%)	NA	NA
Ludmir et al.[34]	2019	Carboplatin – vincristine (19 proton, 9 photon) Temozolomide (5 proton, 0 photon) Vinblastine (4 proton, 0 photon) Other (7 proton, 2 photon)	NA	NA	NA
Harrabi et al.[22] Bahn et al.[23]	2020	ND	NA	NA	NA
Ritterbush et al.[32]	2021	Procarbazine - lomustine - vincristine Temozolomide	NA	NA	NA
Harreld et al.[30]	2022	NA	NA	ND	NA
Eichkorn et al.[21]	2022	ND	NA	ND	Vincristine - lomustine - procarbazine Temozolomide Other
Upadhyay et al.[38]	2022	ND (34%) High dose chemotherapy with stem cell rescue (12%)	ND (25%)	NA	NA

*The detailed version of the high dose chemotherapy regimen is shown in Table S5 (supplementary data)

**Some patients received chemotherapy at multiple times (before and/or during and/or after RT). Therefore, the sum of patients does not correspond to the total number of 52 patients in the population. 16 patients did not receive chemotherapy.

Abbreviations: ND, not defined; NA, not applicable; RT, radiotherapy

Table 12. Timing to radiotherapy

Author[reference]	Year	Surgery to start RT (range) [months]	Surgery to completion of RT (range) [months]	Diagnosis to start RT (range) [months]
Gunther et al.[20]	2015	(0.6-8.0)	ND	ND
Uh et al. [18]	2015	Median 3.2 (0.5-45.6)	ND	ND
Kralik et al.[27]	2015	ND	Median 2.4 (1.1-14.3)	ND
Devine et al.[43]	2019	ND	Median 2.5 (1.4-29.3)	ND
Eichkorn et al.[21]	2022	ND	ND	Median 3.1 (2.0-20.4)

Abbreviations: ND, not defined; RT, radiotherapy

Table 13. Definitions of imaging changes

Author[reference]	Year	Imaging change	Definition
Fouladi et al.[29]	2004	White matter lesion	Grade 1, abnormal signal intensity on T2-weighted images; grade 2, increased signal intensity on T2-weighted images and contrast enhancement on T1; grade 3, evidence of haemorrhage; grade 4, encephalomalacia or focal necrosis.
Sabin et al.[19]	2013	ND	ND
Indelicato et al.[40]	2014	Brainstem toxicity	New or progressive symptoms involving cranial nerves V-VII or IX-XII, motor weakness, or dysmetria with a corresponding radiographic abnormality within the brainstem in the absence of disease progression.
Gunther et al.[20]	2015	ND	Grade 1, abnormal signal intensity on T2-weighted images; grade 2, increased signal intensity on T2-weighted images and contrast enhancement on T1; grade 3, evidence of haemorrhage; grade 4, encephalomalacia or focal necrosis.
Kralik et al.[27]	2015	RN	1) A new area of contrast enhancement occurs in the brain parenchyma, which did not demonstrate abnormal signal or enhancement before radiation therapy. 2) The enhancement must either spontaneously decrease or resolve within 6 months of development on follow-up MR imaging without additional tumour treatment intervention and without evidence of an alternate etiology (i.e., stroke, haemorrhage, or infection) in conjunction with a review of clinical records performed by a board-certified paediatric neuro-oncologist. 3) The area of enhancement is confirmed to be within an area receiving a radiation dose by a board-certified paediatric radiation oncologist.
Plimpton et al.[31]	2015	RN	MRI findings indicative of RN include increasing peritumoral oedema and heterogeneous enhancement.
Giantsoudi et al.[42]	2016	Radiation injury	New or progressive CNS symptoms not attributable to tumour progression. Areas of MRI radiographic changes in asymptomatic patients were not reported as radiation injury.
Peeler et al.[25]	2016	ND	T2-FLAIR hyperintensity with or without enhancement on T1 post-contrast sequences.
Gentile et al.[39]	2018	Brainstem injury	New or progressive CNS symptoms not attributable to tumour progression. Areas of MRI radiographic changes in asymptomatic patients were not reported as radiation injury.
Hall et al.[35]	2018	Vasculopathy	Any asymptomatic vessel narrowing identified on imaging or found after symptomatic presentations from transient ischemic attacks or CVA.
Hall et al.[35]	2018	Serious vasculopathy	Any vascular anomaly resulting in permanent neurologic deficits or that required revascularization surgery.
Kralik et al.[37]	2018	Cerebral microbleed	An intraparenchymal small (≤ 5 mm) round or ovoid hypointensity on SWI imaging that did not correspond to vessels or tumour, that did not border the surgical resection site or expected location of mineralization, and that was not hyperintense on T1-weighted or T2-weighted imaging.
Kralik et al.[37]	2018	Cavernous malformation	A round or ovoid hypointensity on SWI that demonstrated hyperintense T1-weighted and/or T2-weighted appearance.
Bjoaxhiu et al.[28]	2018	RN	Increased signal intensity on T2-weighted images and new contrast enhancement on T1 occurring in the brain parenchyma included in the radiation treatment field, which did not demonstrate any abnormality before proton RT.
Bjoaxhiu et al.[28]	2018	White matter lesion	Abnormal signal intensity on T2-weighted images occurring in the brain parenchyma included in the radiation treatment field, which did not demonstrate any abnormality before proton RT.
Roberts et al.[45]	2019	RIC	T1 post-contrast or T2 FLAIR changes outside of the gross tumour volume.
Devine et al.[43]	2019	Brainstem injury	New post-RT FLAIR/T2 lesions in the brainstem and findings consistent with radiation necrosis (ring, irregular enhancement within brainstem lesions)
Ludmir et al.[34]	2019	PsP	Bidirectional product (in mm^2) of the solid component of tumour increased by at least 5% of the original pre-RT volume, and the lesion either remained stable or subsequently decreased in size for at least 12 months without new oncologic therapy.

Table 13. Definitions of imaging changes *(continued)*

Harrabi et al.[22]	2020	RICE	ND
Bahn et al.[23]	2020	RICE	Localization within the brain tissue and outside of the gross tumour volume.
Ritterbush et al.[32]	2021	ProPsP	Located at the distal end of the proton beam, resolves without tumour-directed therapy, multifocal, patchy, and small (< 1cm).
Harreld et al.[30]	2022	Subacute RN	Subacute: up to 1 year after completion of RT. RN: New brain parenchymal enhancement within the radiation field that improved or resolved without additional cancer-directed therapy.
Eichkorn et al.[21]	2022	RICE	New post-treatment contrast enhancement on MRI in surrounding brain tissue within the 80% isodose analogous to RANO criteria during the follow-up period.
Fredrik Fjæra et al.[41]	2022	Symptomatic brainstem toxicity	New or progressive symptoms not attributable to tumour progression, and further characterized as grade 2+ response according to the CTCAE version 4.0
Upadhyay et al.[38]	2022	Symptomatic brainstem injury	New or progressive cranial neuropathy (V–VII or IX–XII), bulbar weakness, ataxia, dysmetria, and/or motor weakness with corresponding radiographic abnormality within the brainstem, and absence of any evidence of disease progression

Abbreviations: RN, radiation necrosis; RIC, radiation-induced changes; PsP, pseudoprogression; ProPsP, proton pseudoprogression; RICE, radiation-induced contrast enhancement; CNS, central nervous system; MRI, magnetic resonance imaging; SWI, susceptibility-weighted imaging; RT, radiotherapy; RANO, Response Assessment in Neuro-Oncology; CTCAE, Common Terminology Criteria for Adverse Events

Table 14. Imaging changes

Author[reference]	Year	MRI imaging change	Time to onset (range) [months]	Time to regression (range) [months]	Overall cohort	Patients with imaging changes (% of overall cohort)	Patients with symptomatic imaging changes (% of overall cohort)
Fouladi et al.[29]	2004	White matter lesion	Median 7.8 (1.9-13.0)	Median 6.2 (1.68-23.5) (73%)	127	22 (17%)	3 (2.4%)
Sabin et al.[19]	2013	T2/FLAIR hyperintensity T1 hypointensity	Median 3.9 (3.2-6.3)	Median 2.3 (1.5-3.5)	17	8 (47%)	4 (24%)
Indelicato et al.[40]	2014	Brainstem injury	Median 3 (2-12)	ND	313	11 (3.5%)	11 (3.5%)
Gunther et al.[20]	2015	Grade 1 Grade 2 Grade 3 Grade 4	Proton median 3.8 Photon median 5.3	NA	72	Total 16 proton (43%) Total 6 photon (17%) Grade 1: 7 (6 proton, 1 photon) Grade 2: 9 (4 proton, 5 photon) Grade 3: 4 (4 proton, 0 photon) Grade 4: 2 (2 proton, 0 photon)	7 (4 proton, 3 photon) (10%)
Kralik et al.[27]	2015	RN	Median 5.0 (3-11)	Median 5.3 (3-12)	52	16 (31%)	4 (8%)
Plimpton et al.[31]	2015	RN	Median 1.2 (0.5-8.0)	ND	101	5 (5%)	3 (3%)
Giantsoudi et al.[42]	2016	ND	Median 9 (8-18)	ND	111	10 (9%)	4 (3.6%)
Peeler et al.[25]	2016	T2/FLAIR hyperintensity ± T1 post-contrast enhancement	ND	ND	34	14 (41%)	ND
Robersten et al.[45]	2019	RIC	Median 2.9 (0.9-4.6)	Median 8.3 (2.8-28.6)	30	7 (23%)	4 (13%)
Ludmir et al.[34]	2019	PsP	ND	ND	51 proton 32 photon	23 proton (45%) 8 photon (25%)	5 proton (10%) 1 photon (3.1%)
Gentile et al.[39]	2018	Brainstem injury	Median 8.5 (5.3-82.3)	ND	216	5 (2.3%)	5 (2.3%)
Hall et al.[35]	2018	Vasculopathy	ND	ND	644	41 (6.4%)	ND
Hall et al.[35]	2018	Serious vasculopathy	ND	ND	644	17 (2.6%)	ND
Kralik et al.[37]	2018	Cerebral microbleed	Median 8 (3-28)	NA	100	± 80%	ND
Kralik et al.[37]	2018	Cavernous malformation	Median 46 (14-72)	ND	100	4 (4%)	ND
Bojaxhiu et al.[28]	2018	RN	Median 5 (1-26)	Median 6 (1-32)***	171	29 (17%)	12 (7%)
Bojaxhiu et al.[28]	2018	White matter lesion	Median 14.5 (2-62)	Median 9.5 (4-68)***	171	18 (11%)	5 (3%)
Devine et al.[43]	2019	Brainstem necrosis	(3.9-5.7)	(5.3-25.2)	107	2 (1.9%)	0 (0%)
Harrabi et al.[22]	2020	RICE	Median 15	ND	110	31 (28%)	7 (6.4%)
Bahn et al.[22]	2020	RICE	ND	ND	110	23 (21%)	ND
Ritterbush et al.[32]	2021	ProPsP T1 post-contrast enhancement FLAIR post-contrast enhancement	Mean 15.4 (7-27)	Mean 8.7	57 proton 43 photon	14 proton (27%) 0 photon	9 proton (16%) 0 photon
Harreld et al.[30]	2022	RN	Mean 4.8 (1.1-8.5)	Mean 5 (1.6-12)	95	23 (24%)	3 (3.2%)
Eichkorn et al.[21]	2022	RICE	Median 16.9 (1.7-57.2)	ND	227	49 (22%)	27 (12%)
*Eichkorn et al.[21]	2022	RICE	Median 33.2 (9.1-57.2)	ND	42	2 (5%)	1 (2.4%)
**Eichkorn et al.[21]	2022	RICE	Median 16.9 (1.7-40.9)	ND	185	47 (26%)	26 (14%)
Upadhyay[38]	2022	Brainstem injury	Median 6 (3-72)	ND	468	66 (14%)	15 (3.2%)

*Paediatric subpopulation
**Adult subpopulation
***Time to stabilization/ resolution. The value of this time response is decreased because time to stabilization and time to resolution were not distinguished (28)
Abbreviations: ND, not defined; MRI, magnetic resonance imaging; PsP, pseudoprogression; RN, radiation necrosis; ProPsP, proton pseudoprogression; RICE, radiation-induced contrast enhancement

Table 15. Patients with CTCAE grade 5

Author[reference]	Year	Cause	Age (years)	Tumour histology	Tumour location	RT dose (Gy (RBE))	Brainstem D_{max} (Gy (RBE))	Brainstem D_{mean} (Gy (RBE))	Brainstem D_{50} (Gy (RBE))	Chemotherapy
Indelicato et al.[40]	2014	Brainstem toxicity	7.5	Ependymoma	Posterior fossa	59.4	ND	51.1	59.1	ND
Gunther et al.[20]	2015	Brainstem RN	1.3	Ependymoma	Posterior fossa	54.0	ND	39.2	57.0	Yes (after RT)
Bjoaxhiu et al.[28]	2018	Brainstem RN	2.9	Ependymoma grade 3	Posterior fossa	59.4	ND	ND	ND	Yes
Bjoaxhiu et al.[28]	2018	Brainstem RN	2.8	Malignant ectomesenchymoma	Posterior fossa	54.0	ND	ND	ND	Yes
Upadhyay et al.[38]	2022	Brainstem injury	1.3	Ependymoma	Posterior fossa	54.0	55.71	39.17	ND	ND
Upadhyay et al.[38]	2022	Brainstem injury	2.7	Medulloblastoma	Posterior fossa	54.0	56.63	55.74	ND	ND

*MRI performed before surgery and proton RT showed an infarcted region of the pons

Table 16. Clinical variables associated with imaging changes

Author[reference]	Year	Statistically significant	Not statistically significant
Fouladi et al.[29]	2004	NA	Age, risk group, cumulative dose of cyclophosphamide, number of grade 3 or 4 episodes of infections or hypotension, grade 3 or 4 nonhematologic toxicities, diagnosis (medulloblastoma versus others), M stage
Sabin et al.[19]	2013	NA	NA
Indelicato et al.[40]	2014	Age < 5 years Posterior fossa tumour location Specific dosimetric parameters	Sex, race, presence of hydrocephalus, need for a CSF shunt, number of operations prior to RT, extent of resection, use of any chemotherapy, use of intrathecal or high-dose intravenous methotrexate, use of a craniospinal RT component, and use of a mixed modality (proton + photon) treatment plan
Gunther et al.[20]	2015	Age ≤ 3 years Proton RT	Sex, tumour location (infratentorial vs. supratentorial), diagnosis, extent of surgery, total dose
Kralik et al.[27]	2015	AT/RT histology Multiple (>3) chemotherapeutic agents	Age (≤ 2 years or ≤ 3 years), sex, GTR, medulloblastoma histology, ependymoma histology, infratentorial tumour location, pineal tumour location, craniospinal radiation, total dose
Plimpton et al.[31]	2015	NA	Age, radiation dose, chemotherapy and PTV
Peeler et al.[25]	2016	Max LET in CTV > 2.5 keV/µm	Age at RT, time before RT, mean LET in CTV, mean CTV physical dose, max CTV physical dose
Hall et al.[35]	2018	Age < 5 years (multivariate) D_{max} to the optic chiasm ≥ 54 Gy (multivariate)	Extent of surgical resection, chemotherapy, neurofibromatosis, total dose and dose delivered to the optic nerves, chiasm and hypothalamus (multivariate)
Kralik et al.[37]	2018	Younger age Higher D_{max} Higher percentage and volume of the brain exposed to ≥ 30 Gy	Chemotherapy
Bojaxhiu et al.[28]	2018	Ependymoma histology (univariate) Chemotherapy (univariate) Hydrocephalus before RT (univariate)	Age, grade, surgery, concomitant chemotherapy, adjuvant chemotherapy, irradiated volume, total dose (univariate)
Robersten et al.[45]	2019	Younger age (univariate) ≥ 56.6 Gy to the brainstem (univariate)	Age, sex, histology, extent of surgery, concurrent chemotherapy, V55 ≥ 17.7%, dose, presentation (primary vs. recurrent), IMPT specific parameters (univariate)
Ludmir et al.[34]	2019	RT dose (multivariate) RT modality (multivariate) Histology (univariate)	Age, sex, grade, tumour location, extent of pre-RT surgical resection, pre-RT chemotherapy and CTV size (univariate)
Ritterbush et al.[32]	2021	NA	Sex, grade, IDH mutation, MGMT promotor, 1p/19q codeletion status or by chemo therapy received (PCV or temozolomide)
Harrabi et al.[22] Bahn et al.[22]	2020	Proximity to the ventricles LET_D	NA
Harreld et al.[30]	2022	Pretreatment supratentorial white matter MTR	Age, sex, M stage, tumour subtype, treatment risk stratum, visible brain metastases, proton or proton RT
Eichkorn et al.[21]	2022	WHO grade 2 vs.1(multivariate – independent of age and dose but not of IDH mutational status) Older age (multivariate)	Total dose, dose per fraction, number of beams, CTV volume, dose at the ventricular system and anatomical localization of tumours, adjusted for age. (multivariate)
Upadhyay[38]	2022	Age ≤3 years (univariate) Female gender (multivariate) AT/RT histology (univariate) High-dose chemotherapy with stem cell rescue (multivariate) No craniospinal irradiation (multivariate) Higher V_{50-52}	Infratentorial location, hydrocephalus, extent of resection (GTR), multiple resections, timing of RT (before 2014), chemotherapy, posterior fossa syndrome,

Abbreviations: NA, not applicable; RT, radiotherapy; MTR, magnetization transfer ratio; WHO, world health organization; IDH, isocitrate dehydrogenase; AT/RT, atypical teratoid/rhabdoid tumour; CSF, cerebrospinal fluid; D_{max}, maximum dose; PCV, procarbazine, lomustine and vincristine; CTV, clinical target volume

4 Discussion

Several studies have shown a higher incidence of imaging changes after proton versus photon RT. In this thesis we focused on the question whether and which of these imaging changes are clinically relevant and more specifically their possible causes.

4.1 Imaging changes

Several studies describe the occurrence of imaging changes, the definitions of which are given in Table 13. This table shows that the observed imaging changes are not defined homogeneously or unequivocally. The literature mainly refers to PsP and RN. However, there is overlap in both terminology and appearance of these imaging changes.

4.1.1 Pseudoprogression

PsP is a subacute imaging change after RT that spontaneously regresses over time. It is crucial to distinguish PsP from true tumour progression to avoid inappropriate treatment interventions (33). This distinction is challenging because the contrast enhancement observed in PsP is similar to that observed in tumour progression (32). Therefore, criteria have been established to allow this differential diagnosis (46). These criteria are based on timing and location of PsP after photon RT. However, PsP develops later after proton compared to photon RT (32, 33). Therefore, it could be incorrectly considered as tumour progression according to current guidelines. In addition to differences in timing, Ritterbusch et al. (32) also observed differences in the appearance and area of PsP after proton and photon RT. Consequently, the authors established criteria to characterize proton PsP.

Furthermore, the incidence of PsP should also be considered. One study (34) suggested a higher rate of PsP after proton compared to photon RT. In contrast, a large meta-analysis (47) found no differences in the PsP rates between the RT modalities, which was supported by a recent retrospective study (33). These data are rather controversial and there is no general agreement on the appearance of PsP after RT indicating that more research will be required.

4.1.2 Radiation necrosis

During RT, the most feared treatment complication is RN. The golden standard to diagnose this complication is biopsy (48). However, it is not generally performed since the surgical intervention needed for biopsy is associated with an increased morbidity or even mortality risk. Consequently,

several imaging modalities are used as an alternative (27). Nevertheless, on imaging the distinction between RN and tumour progression is not always clear.

Several studies reported RN rates after proton RT ranging from 17% up to 31% (27, 28, 30). In contrast, one study (31) reported RN after photon RT with an incidence rate of 5%. These findings suggest a higher rate of RN after proton compared to photon RT. However, most studies focus on imaging changes in general rather than RN, making it difficult to assess the true incidence of RN. Furthermore, the time to onset of RN should be considered. From the data collected in Table 14, it is apparent that the median time to onset of RN is later after proton compared to photon RT (5 months vs. 1.2 months). However, a wide range from months to years has been reported (27, 28, 30). Taken together, further research is recommended to estimate the real incidence and timing of RN after proton and photon RT.

4.1.3 Brainstem injury

After RT the most feared treatment complication is RN, especially in the brainstem. The brainstem is important for the regulation of many vital functions. Damage to the brainstem is therefore a severe and potentially lethal complication (14). Indeed, from the data collected in Table 15, it is apparent that all patients with grade 5 brain toxicity had brainstem injury.

A recent study (38) of a large paediatric cohort reported a 14% incidence of brainstem injury after proton RT. When only considering symptomatic brainstem injury, a lower incidence of 3.2% was reported which is comparable to two other large studies (2.3% and 3.5%) (39, 40). In contrast, Devine et al. (43) reported a 1.9% incidence of brainstem injury after photon RT. The authors adapted dosimetric parameters which were previously shown to correlate with a brainstem injury rate of 10.5% after proton RT (40). However, several limitations might have contributed to this low rate (1.9%), including small sample size, limited follow-up period and exclusion of patients with tumours infiltrating the brainstem. These findings suggest a higher risk of brainstem injury after proton compared to photon RT. Since most studies lack a direct photon or proton comparison arm, further research is needed to confirm this finding.

4.2 Symptomatic versus asymptomatic

Both PsP and RN can be either symptomatic or asymptomatic. Although most imaging changes remain asymptomatic, some of them cause severe symptoms requiring surgical intervention. The most feared treatment complication is mortality. To understand the clinical relevance of imaging changes it is essential to report both symptomatic and asymptomatic changes. However, some studies describe only symptomatic changes (39, 40, 42). Certain studies are also inconsistent in

referring asymptomatic and symptomatic patients separately. For instance, Giantsoudi et al. (42) first describe 10 patients with imaging changes, 4 of which developed symptoms. However, later in their results they mention 10 symptomatic imaging changes. This reporting error was adopted in another study (36) that referred to the study of Giantsoudi et al.

The CTCAE is used as standard classification for adverse events. This classification allows the comparison of studies with respect to the severity of reported adverse events. However, this comparison is not feasible when the CTCAE is applied incorrectly. For instance, Eichkorn et al. (21) reported 23 patients with grade 0. However, according to the CTCAE v4.0 (13), a grade 0 does not exist. What the authors consider as grade 0 is not explained. When analysing their data, we suspect that grade 0 refers to the asymptomatic patients whereas grade 1 refers to the patients with mild symptoms. According to the CTCAE both should be considered as grade 1. Furthermore, no imaging changes were classified as grade 2 because all patients with symptoms requiring treatment were classified as grade 3. It is rather unconventional to classify patients in a higher toxicity grade without good explanation or justification. Thus, no distinction can be made between patients with moderate and severe symptoms.

4.3 Radiotherapy

4.3.1 Proton versus photon radiotherapy

Proton RT is less robust to anatomical changes during treatment (17). However, only two studies (20, 34) compared the development of imaging changes between patients treated with proton RT and patients treated with photon RT. In both studies, proton RT was associated with an increased risk of imaging changes.

4.3.2 Delivery technique

The two major delivery techniques in proton RT are PS and PBS. Most patients receiving proton RT have been treated with PS as this is the oldest proton delivery technique. However, high-dose areas or “dose hotspots” appear to occur more frequently during PS due to increased dose heterogeneity (34, 47). Current treatment facilities use PBS because of its dosimetric advantages. However, increasing the spot distance may lead to additional dose outside the PTV (16).

Taken together, these findings suggest that the delivery technique may contribute to the development of imaging changes. However, the delivery technique is not defined in one-third of the studies, as shown in Table 10. It is unclear from our results whether rates of imaging changes differ between patients treated with PBS and those treated with PS. Further research is needed to clarify this difference.

4.3.3 Radiation dose

When discussing radiation dose, both physical and biological dose should be considered. The physical dose is the total radiation dose absorbed by the irradiated tissue, whereas the biological dose is that part of the physical dose that causes a biological effect in the irradiated tissue.

4.3.3.1 Physical dose

In treatment planning, the physical dose is known as the total prescribed dose. Only Ludmir et al. (34) indicated an increased dose (> 50.4 Gy) as a predictor for the development of PsP. In contrast, other studies could not establish a significant correlation between the total dose and imaging changes. Moreover, we noticed that the median dose in the study of Ludmir et al. was lower than the median dose in all the other studies that did not find a correlation (50.4 Gy vs. 54.0-59.4 Gy). These controversial findings could be due to the different reported imaging changes among the studies. Ludmir et al. reported PsP while the other studies reported RN or general MRI changes. Taken together, we assume that PsP could develop at lower doses than RN or general MRI changes. However, this assumption is not supported by the study of Stock et al. (33) that found no differences in PsP rates when comparing low radiation doses (≤ 50.4 Gy) with high doses (> 50.4 Gy).

In addition to total dose, several other dosimetric parameters (e.g., D_{max}, D_{50}, V_{55}) have been indicated as potential risk factors for the development of imaging changes (20, 36-40). However, studies report different significant values for these dosimetric parameters. For instance, two studies (20, 40) reported that brainstem D_{50} > 52.4 Gy or D_{50} ≥ 54 Gy was associated with imaging changes. These values show a similar trend but are not identical. However, specific values are necessary for implementation in clinical practice. Therefore, randomized trials should provide more uniform evidence. The only conclusion we can draw from these findings is that dosimetric parameters are contributing factors to the development of imaging changes.

4.3.3.2 Biological dose

In proton treatment planning, the RBE is used to convert the physical dose into a biological effective dose. In current clinical practice, a fixed RBE value of 1.1 is used. However, preclinical and clinical data suggest significant variations of the RBE along the SOBP (24, 49). The RBE increases at the distal end of the proton beam due to increasing LET (22, 50). This causes an uncertainty in the delivered biological effective dose. Therefore, tissue toxicity may occur within or immediately

adjacent to the region of elevated RBE weighted dose. Consequently, the Bragg-peak is currently no longer placed close to critical structures to avoid tissue toxicity due to RBE uncertainty (35, 40).

In recent years, several studies have tried to determine the clinical relevance of a variable RBE in terms of imaging changes or tissue toxicity. Multiple published studies have found a correlation between imaging changes and LET/RBE (23, 25, 36) while others have not been able to identify a significant correlation (42, 51, 52).

There is an important distinction between physical and biological dose. Using a biological dose model in treatment planning may better predict dose hot spots in critical structures (45). RBE and LET must be considered to estimate the real biological effective dose and thus the real risk of imaging changes. However, the use of variable RBE values is currently not feasible due to uncertainties about the conversion factors (24). Since variations in RBE along the SOBP are assumed to be one of the main causes of unexpected tissue toxicity, it is strongly recommended that further research focuses on how to implement these variable RBE. This is crucial to optimize treatment planning and reduce toxicity risks.

4.4 Adjuvant treatment

There are three treatment modalities for CNS tumours: surgery, radiotherapy and chemotherapy. The combined effect of these treatment modalities is considered as a potential cause of imaging changes (19). Therefore, we discuss our findings regarding the impact of surgery and chemotherapy on radiation-induced imaging changes.

4.4.1 Surgery

Surgery is often the first-line treatment for CNS tumours. However, some studies identify surgery as a risk factor for imaging changes. Surgical defects present at the time of RT enhance the radiation dose effect (18). This suggests that surgery-affected regions are less resilient to radiation. However, these authors mentioned the time from surgery to RT as a potential confounding factor for their findings. Another study observed that a shorter interval between surgery and RT trended towards a higher risk of imaging changes (20). This may be due to insufficient tissue healing after surgery and consequently, resulting in the presence of surgical defects at the time of RT. Therefore, the interval between surgery and RT should be taken into account. However, few studies mention this interval as shown in Table 12. Additionally, Indelicato et al. (40) suggest more conservative dosimetric guidelines for young patients with posterior fossa tumours, particularly those undergoing aggressive surgery.

4.4.2 Chemotherapy

Although many chemotherapeutic agents sensitize tumour cells to radiation, the contribution of chemotherapy to radiation-induced imaging changes remains poorly understood (40). Several studies have found a correlation between imaging changes and chemotherapy (27, 28, 38, 39), while others were unable to identify a significant correlation. Kralik et al. (27) found that the combination of multiple (> 3) chemotherapeutic agents was a risk factor for the development of RN. However, the impact of individual agents on the development of RN was not determined. Other studies (38, 39) reported high-dose chemotherapy with stem cell rescue as a significant predictive factor for brainstem injury. In contrast, Gunther et al. (20) observed that patients treated with chemotherapy trended towards a lower risk of imaging changes. In these patients, the administration of chemotherapy obviously prolonged the start of RT, resulting in a longer interval between surgery and RT. This longer interval probably enabled tissue repair after surgery, which could explain this contradictory finding. Although these findings are relevant, implementation in clinical practice is challenging due to insufficient specifications. Most studies do not provide detailed information on the chemotherapeutic regimen, such as chemotherapeutic agents, dose and administration before or during RT. The lack of these details is highlighted in Table 11.

4.5 Patient characteristics

4.5.1 Tumour

CNS tumours include several different tumour histological subtypes. Some of these tumours, such as AT/RT (27, 38) or ependymoma (28), are indicated as a potential risk factor for the development of imaging changes. However, for patients with AT/RTs this correlation could be due to the high-dose chemotherapy being part of their treatment (cf. 4.4.2). Furthermore, for patients with ependymomas this correlation could be due to the higher dose given to tumours with a higher WHO grading. Current guidelines recommend a radiation dose of 54 Gy in WHO grade I and II ependymomas, whereas 59.4 Gy is recommended in WHO grade III ependymomas. Moreover, a major drawback of patient cohort studies is that the number of different tumour histologies were relatively small. Kralik et al. (27) observed RN in all patients with AT/RTs. The authors found a significant correlation between AT/RT histology and imaging changes. However, their conclusion is based on only 3 patients.

On the other hand, for patients with ependymomas, the correlation with imaging changes could be due to the tumour location rather than the tumour histology since two-thirds of ependymomas originate in the posterior fossa. This posterior fossa tumour location is associated

with an increased risk of brainstem injury (40). Based on this finding, we assumed that studies examining only posterior fossa tumours would report a higher incidence of brainstem injury. In contrast, Gentile et al. (39) and Devine et al. (43) reported a low rate of brainstem injury (2.3% and 1.9%, respectively). In the study by Gentile et al, this low rate could be an underestimation since only symptomatic brainstem injury was investigated. Devine et al. mentioned several limitations that might have contributed to their low rate of brainstem injury (cf. 4.1.3). Furthermore, from the data collected in Table 15, it is apparent that all patients with grade 5 toxicity were treated for posterior fossa tumours.

In addition to the posterior fossa, two studies reported that imaging changes are more likely to occur periventricularly (22, 23). This suggests an increased periventricular radiation sensitivity. These areas could be more vulnerable due to their terminal blood supply, as a reduced blood supply is associated with a reduced tissue repair capacity (23).

These findings suggest that the correlation between imaging changes and tumour location is more convincing than the correlation with tumour histology.

4.5.2 Age

In neuro-oncology, the patient's age is crucial for treatment. To reduce the risk of RT-associated neurocognitive decline, RT will often be delayed in infants or very young patients (1). This means that the interval between the time of diagnosis and the start of RT might be longer than expected for some tumour histologies. For instance, in a very young patient (< 3 years) with medulloblastoma, CSI is delayed and replaced by chemotherapy to reduce long-term neurotoxicity, while in a similar patient with an ependymoma, local RT will be given. To investigate possible correlations between the patient's age and the development of radiation-induced imaging changes, it is important to report both the age at diagnosis as well as the age at RT. Unfortunately, some authors (43) only mention the age at diagnosis.

Several studies found a correlation between imaging changes and younger age (37) while others did not find any significant link. Age ≤ 3 years (20, 38) and age < 5 years (35, 40) have been identified as significant risk factors for the development of imaging changes. In contrast, one study (21) concluded that older age (i.e., adults vs. children) is associated with subsequent development of radiation-induced imaging changes. This study reported MRI changes in general, whereas all other studies described symptomatic imaging changes and vascular damage. A putative explanation for these contradictory findings is that the severity of imaging changes in children is

more relevant than the amount of imaging changes. In addition, vascular structures might be more sensitive in children.

Taken together, we conclude that age is not an independent risk factor for the development of imaging changes (symptomatic and/or asymptomatic). However, the sensitivity of the paediatric brain to treatment-induced damage is well known. Consequently, in treatment planning, it is still crucial to consider the patient's age.

4.5.3 Individual radiosensitivity

Little is known about the normal tissue tolerance of the CNS in paediatric patients (53). Unknown genetic differences might increase radiosensitivity, resulting in a higher susceptibility to MRI changes after RT. Harreld et al. (30) describe decreased myelin density as a potential predictive factor for RN. This decrease might be due to genetic differences. Although genetic predisposition could be an important predictive factor for the development of imaging changes, implementation of this information in treatment planning is challenging.

4.6 Limitations of the clinical studies

Several limitations of the clinical studies need to be considered. First, a major challenge within this topic is the small sample size of the studies due to the low incidence of paediatric CNS tumours. Consequently, the findings within the articles were often not statistically significant. Moreover, the power of statistical analysis is often limited by the limited number of events. Because of the small sample sizes, the findings may not be extrapolated to all paediatric patients.

Second, most studies are limited by their retrospective design. By retrospectively compiling a patient cohort, selection bias may occur and needs to be considered when interpreting clinical outcomes. Moreover, many studies lack a direct photon or proton comparison arm and compare their results with data from historic cohorts.

Third, in most studies there is missing information of patient and treatment details. Some patients are lost to follow-up which may result in an underestimation of true incidence rates. Finally, differences in clinical terminology lead to varying estimates mainly because the radiologic definitions of MRI lesions after RT are not defined homogeneously.

4.7 Limitations to this literature research

This master's thesis had several challenges. The main difficulty of this master's thesis was the complexity of the subject. Therefore, having a detailed knowledge of general principles of RT was necessary. Furthermore, comparing the reported data was challenging due to study heterogeneity. To come to a structured overview of patient characteristics, treatment details and imaging changes, this data was summarized in Tables 10 to 16. These tables were of added value to write our discussion. By generating our tables we found out that detailed information is missing in several studies, which is not always clear when reading the individual studies.

5 Conclusion and perspectives

Several studies have shown a higher incidence of imaging changes after proton versus photon RT. In this thesis we focused on the question whether and which of these imaging changes are clinically relevant and more specifically their possible causes. The literature mainly refers to the development of PsP and RN after RT. Both imaging changes can be symptomatic, which is clinically relevant. However, PsP spontaneously regresses over time, while RN is considered as irreversible damage. Therefore, RN is indicated as the most feared treatment complication after RT. Especially RN of the brainstem is of concern as it is also associated with a mortality risk. However, there is overlap in both terminology and appearance of PsP and RN which makes it difficult to draw definite conclusions from the literature studied.

Our main finding is that the development of MRI changes is multifactorial. Both patient- and treatment-related factors should be considered to minimise the risk of imaging changes. Therefore, further research is recommended to better understand the impact of these individual factors and their interactions. This is necessary to optimise the safety of treatment planning. For instance, the variable RBE is not incorporated in clinical treatment planning due to uncertainties in published RBE values. However, this variable RBE is assumed to be one of the main causes of unexpected tissue toxicity after proton RT. Therefore, understanding of the RBE needs to be improved to enable implementation in clinical practice.

Whether long-term advantages of proton therapy outweigh the risks of complications deserves further investigation. Randomised controlled trials comparing proton versus photon would be the golden standard. However, it is ethically very difficult to include children in trials where they may receive treatment with a higher risk of toxicity.

Finally, further research should report complete patient characteristics and treatment details in a uniform way to enable comparison of study results.

6 References

1. Tom Boterberg KD, Mark Gaze. Radiotherapy and the Cancers of Children, Teenagers, and Young Adults: Oxford university press; 2021.
2. Preston DC. Magnetic Resonance Imaging (MRI) of the Brain and Spine: Basics 2016. Available from: https://case.edu/med/neurology/NR/MRI%20Basics.htm.
3. Belgian Cancer Register. Available from: http://kankerregister.org/.
4. Louis DN, Perry A, Wesseling P, Brat DJ, Cree IA, Figarella-Branger D, et al. The 2021 WHO Classification of Tumors of the Central Nervous System: a summary. Neuro Oncol. 2021;23(8):1231-51.
5. Lamba N, Groves A, Torre M, Yeo KK, Iorgulescu JB. The epidemiology of primary and metastatic brain tumors in infancy through childhood. J Neurooncol. 2022;156(2):419-29.
6. Fjæra LF. Studies of the linear energy transfer and relative biological effectiveness in proton therapy of pediatric brain tumors: University of Bergen; 2021.
7. Paganetti H, Kooy H. Proton radiation in the management of localized cancer. Expert Rev Med Devices. 2010;7(2):275-85.
8. Fotontherapie versus protontherapie. www.particle.be.
9. McMahon SJ. The linear quadratic model: usage, interpretation and challenges. Phys Med Biol. 2018;64(1):01tr.
10. Sørensen BS, Pawelke J, Bauer J, Burnet NG, Dasu A, Høyer M, et al. Does the uncertainty in relative biological effectiveness affect patient treatment in proton therapy? Radiother Oncol. 2021;163:177-84.
11. RIZIV. Available from: https://www.riziv.fgov.be/nl/professionals/verzorgingsinstellingen/ziekenhuizen/zorg/Paginas/hadrontherapie.aspx
12. Yock TI, Bhat S, Szymonifka J, Yeap BY, Delahaye J, Donaldson SS, et al. Quality of life outcomes in proton and photon treated pediatric brain tumor survivors. Radiother Oncol. 2014;113(1):89-94.
13. Cancer Therapy Evaluation Program 2021 [updated 04/19/2021. Available from: https://ctep.cancer.gov.
14. Lambrecht M, Eekers DBP, Alapetite C, Burnet NG, Calugaru V, Coremans IEM, et al. Radiation dose constraints for organs at risk in neuro-oncology; the European Particle Therapy Network consensus. Radiother Oncol. 2018;128(1):26-36.
15. Mayo C, Yorke E, Merchant TE. Radiation associated brainstem injury. Int J Radiat Oncol Biol Phys. 2010;76(3 Suppl):S36-41.
16. Fjæra LF, Li Z, Ytre-Hauge KS, Muren LP, Indelicato DJ, Lassen-Ramshad Y, et al. Linear energy transfer distributions in the brainstem depending on tumour location in intensity-modulated proton therapy of paediatric cancer. Acta Oncol. 2017;56(6):763-8.
17. Lassen-Ramshad Y, Vestergaard A, Muren LP, Høyer M, Petersen JB. Plan robustness in proton beam therapy of a childhood brain tumour. Acta Oncol. 2011;50(6):791-6.
18. Uh J, Merchant TE, Li Y, Li X, Sabin ND, Indelicato DJ, et al. Effects of Surgery and Proton Therapy on Cerebral White Matter of Craniopharyngioma Patients. Int J Radiat Oncol Biol Phys. 2015;93(1):64-71.
19. Sabin ND, Merchant TE, Harreld JH, Patay Z, Klimo P, Jr., Qaddoumi I, et al. Imaging changes in very young children with brain tumors treated with proton therapy and chemotherapy. AJNR Am J Neuroradiol. 2013;34(2):446-50.
20. Gunther JR, Sato M, Chintagumpala M, Ketonen L, Jones JY, Allen PK, et al. Imaging Changes in Pediatric Intracranial Ependymoma Patients Treated With Proton Beam Radiation Therapy Compared to Intensity Modulated Radiation Therapy. Int J Radiat Oncol Biol Phys. 2015;93(1):54-63.
21. Eichkorn T, Bauer J, Bahn E, Lischalk JW, Meixner E, Sandrini E, et al. Radiation-induced contrast enhancement following proton radiotherapy for low-grade glioma depends on tumor characteristics and is rarer in children than adults. Radiother Oncol. 2022;172:54-64.
22. Harrabi S, Bauer J, Bahn E, Adeberg S, Haberer T, Alber M, et al. Radiation-Induced Brain Injury after Proton Radiotherapy Is Linked to Increased Distal Edge Linear Energy Transfer (LET) and Anatomically Variable Radiation Sensitivity. International Journal of Oncology Biology Physics. 2019;105(1):E99.
23. Bahn E, Bauer J, Harrabi S, Herfarth K, Debus J, Alber M. Late Contrast Enhancing Brain Lesions in Proton-Treated Patients With Low-Grade Glioma: Clinical Evidence for Increased Periventricular Sensitivity and Variable RBE. Int J Radiat Oncol Biol Phys. 2020;107(3):571-8.

24. Paganetti H. Mechanisms and Review of Clinical Evidence of Variations in Relative Biological Effectiveness in Proton Therapy. Int J Radiat Oncol Biol Phys. 2022;112(1):222-36.
25. Peeler CR, Mirkovic D, Titt U, Blanchard P, Gunther JR, Mahajan A, et al. Clinical evidence of variable proton biological effectiveness in pediatric patients treated for ependymoma. Radiother Oncol. 2016;121(3):395-401.
26. Davanzo J, Greiner RJ, Barbour M, Rizk E. Radiation Necrosis Following Proton Beam Therapy in the Pediatric Population: a Case Series. Cureus. 2017;9(10):e1785.
27. Kralik SF, Ho CY, Finke W, Buchsbaum JC, Haskins CP, Shih CS. Radiation Necrosis in Pediatric Patients with Brain Tumors Treated with Proton Radiotherapy. AJNR Am J Neuroradiol. 2015;36(8):1572-8.
28. Bojaxhiu B, Ahlhelm F, Walser M, Placidi L, Kliebsch U, Mikroutsikos L, et al. Radiation Necrosis and White Matter Lesions in Pediatric Patients With Brain Tumors Treated With Pencil Beam Scanning Proton Therapy. Int J Radiat Oncol Biol Phys. 2018;100(4):987-96.
29. Fouladi M, Chintagumpala M, Laningham FH, Ashley D, Kellie SJ, Langston JW, et al. White matter lesions detected by magnetic resonance imaging after radiotherapy and high-dose chemotherapy in children with medulloblastoma or primitive neuroectodermal tumor. J Clin Oncol. 2004;22(22):4551-60.
30. Harreld JH, Zou P, Sabin ND, Edwards A, Han Y, Li Y, et al. Pretreatment Normal WM Magnetization Transfer Ratio Predicts Risk of Radiation Necrosis in Patients with Medulloblastoma. AJNR Am J Neuroradiol. 2022;43(2):299-303.
31. Plimpton SR, Stence N, Hemenway M, Hankinson TC, Foreman N, Liu AK. Cerebral radiation necrosis in pediatric patients. Pediatr Hematol Oncol. 2015;32(1):78-83.
32. Ritterbusch R, Halasz LM, Graber JJ. Distinct imaging patterns of pseudoprogression in glioma patients following proton versus photon radiation therapy. J Neurooncol. 2021;152(3):583-90.
33. Stock A, Hancken CV, Kandels D, Kortmann RD, Dietzsch S, Timmermann B, et al. Pseudoprogression Is Frequent After Front-Line Radiation Therapy in Pediatric Low-Grade Glioma: Results From the German Low-Grade Glioma Cohort. Int J Radiat Oncol Biol Phys. 2022;112(5):1190-202.
34. Ludmir EB, Mahajan A, Paulino AC, Jones JY, Ketonen LM, Su JM, et al. Increased risk of pseudoprogression among pediatric low-grade glioma patients treated with proton versus photon radiotherapy. Neuro Oncol. 2019;21(5):686-95.
35. Hall MD, Bradley JA, Rotondo RL, Hanel R, Shah C, Morris CG, et al. Risk of Radiation Vasculopathy and Stroke in Pediatric Patients Treated With Proton Therapy for Brain and Skull Base Tumors. Int J Radiat Oncol Biol Phys. 2018;101(4):854-9.
36. Bolsi A, Placidi L, Pica A, Ahlhelm FJ, Walser M, Lomax AJ, et al. Pencil beam scanning proton therapy for the treatment of craniopharyngioma complicated with radiation-induced cerebral vasculopathies: A dosimetric and linear energy transfer (LET) evaluation. Radiother Oncol. 2020;149:197-204.
37. Kralik SF, Mereniuk TR, Grignon L, Shih CS, Ho CY, Finke W, et al. Radiation-Induced Cerebral Microbleeds in Pediatric Patients With Brain Tumors Treated With Proton Radiation Therapy. Int J Radiat Oncol Biol Phys. 2018;102(5):1465-71.
38. Upadhyay R, Liao K, Grosshans DR, McGovern SL, Frances McAleer M, Zaky W, et al. Quantifying the risk and dosimetric variables of symptomatic brainstem injury after proton beam radiation in pediatric brain tumors. Neuro Oncol. 2022;24(9):1571-81.
39. Gentile MS, Yeap BY, Paganetti H, Goebel CP, Gaudet DE, Gallotto SL, et al. Brainstem Injury in Pediatric Patients With Posterior Fossa Tumors Treated With Proton Beam Therapy and Associated Dosimetric Factors. Int J Radiat Oncol Biol Phys. 2018;100(3):719-29.
40. Indelicato DJ, Flampouri S, Rotondo RL, Bradley JA, Morris CG, Aldana PR, et al. Incidence and dosimetric parameters of pediatric brainstem toxicity following proton therapy. Acta Oncol. 2014;53(10):1298-304.
41. Fredrik Fjæra L, Indelicato DJ, Handeland AH, Ytre-Hauge KS, Lassen-Ramshad Y, Muren LP, et al. A case-control study of linear energy transfer and relative biological effectiveness related to symptomatic brainstem toxicity following pediatric proton therapy. Radiother Oncol. 2022.
42. Giantsoudi D, Sethi RV, Yeap BY, Eaton BR, Ebb DH, Caruso PA, et al. Incidence of CNS Injury for a Cohort of 111 Patients Treated With Proton Therapy for Medulloblastoma: LET and RBE Associations for Areas of Injury. Int J Radiat Oncol Biol Phys. 2016;95(1):287-96.
43. Devine CA, Liu KX, Ioakeim-Ioannidou M, Susko M, Poussaint TY, Huisman T, et al. Brainstem Injury in Pediatric Patients Receiving Posterior Fossa Photon Radiation. Int J Radiat Oncol Biol Phys. 2019;105(5):1034-42.

44. Hua C, Merchant TE, Gajjar A, Broniscer A, Zhang Y, Li Y, et al. Brain tumor therapy-induced changes in normal-appearing brainstem measured with longitudinal diffusion tensor imaging. Int J Radiat Oncol Biol Phys. 2012;82(5):2047-54.
45. Roberts KW, Wan Chan Tseung HS, Eckel LJ, Harmsen WS, Beltran C, Laack NN. Biologic Dose and Imaging Changes in Pediatric Brain Tumor Patients Receiving Spot Scanning Proton Therapy. Int J Radiat Oncol Biol Phys. 2019;105(3):664-73.
46. Chukwueke UN, Wen PY. Use of the Response Assessment in Neuro-Oncology (RANO) criteria in clinical trials and clinical practice. CNS Oncol. 2019;8(1):Cns28.
47. Lu VM, Welby JP, Laack NN, Mahajan A, Daniels DJ. Pseudoprogression after radiation therapies for low grade glioma in children and adults: A systematic review and meta-analysis. Radiother Oncol. 2020;142:36-42.
48. Furuse M, Nonoguchi N, Yamada K, Shiga T, Combes JD, Ikeda N, et al. Radiological diagnosis of brain radiation necrosis after cranial irradiation for brain tumor: a systematic review. Radiat Oncol. 2019;14(1):28.
49. Cuaron JJ, Chang C, Lovelock M, Higginson DS, Mah D, Cahlon O, et al. Exponential Increase in Relative Biological Effectiveness Along Distal Edge of a Proton Bragg Peak as Measured by Deoxyribonucleic Acid Double-Strand Breaks. Int J Radiat Oncol Biol Phys. 2016;95(1):62-9.
50. Paganetti H. Relative biological effectiveness (RBE) values for proton beam therapy. Variations as a function of biological endpoint, dose, and linear energy transfer. Phys Med Biol. 2014;59(22):R419-72.
51. Garbacz M, Cordoni FG, Durante M, Gajewski J, Kisielewicz K, Krah N, et al. Study of relationship between dose, LET and the risk of brain necrosis after proton therapy for skull base tumors. Radiother Oncol. 2021;163:143-9.
52. Niemierko A, Schuemann J, Niyazi M, Giantsoudi D, Maquilan G, Shih HA, et al. Brain Necrosis in Adult Patients After Proton Therapy: Is There Evidence for Dependency on Linear Energy Transfer? Int J Radiat Oncol Biol Phys. 2021;109(1):109-19.
53. Dell'Oro M, Short M, Wilson P, Bezak E. Normal tissue tolerance amongst paediatric brain tumour patients- current evidence in proton radiotherapy. Crit Rev Oncol Hematol. 2021;164:103415.

SUPPLEMENTARY

Table S1. 2021 WHO Classification of gliomas (4)

	Subtypes
Adult-type diffuse gliomas	Astrocytoma, IDH-mutant Oligodendroglioma, IDH-mutant, and 1p/19q-codeleted Glioblastoma, IDH-wildtype
Paediatric-type diffuse low-grade gliomas	Diffuse astrocytoma, MYB- or MYBL1-altered Angiocentric glioma Polymorphous low-grade neuroepithelial tumour of the young Diffuse low-grade glioma, MAPK pathway-altered
Paediatric-type diffuse high-grade gliomas	Diffuse midline glioma, H3 K27-altered Diffuse hemispheric glioma, H3 G34-mutant Diffuse paediatric-type high-grade glioma, H3-wildtype and IDH-wildtype Infant-type hemispheric glioma
Circumscribed astrocytic gliomas	Pilocytic astrocytoma High-grade astrocytoma with piloid features Pleomorphic xanthoastrocytoma Subependymal giant cell astrocytoma Chordoid glioma Astroblastoma, MN1-altered

Abbreviations: IDH, isocitrate dehydrogenase

Table S2. Risk stratification for medulloblastoma adapted from (1)

	Low risk	**Standard risk**	**High risk**
Molecular pathology	Mutated β-catenin or positive nuclear β-catenin IHC with monosomy 6	Positive nuclear β-catenin IHC without monosomy 6 or negative nuclear β-catenin IHC	MYC or MYCN amplification
Histopathology	Classical or desmoplastic/nodular	Classical or desmoplastic/nodular	Large cell, anaplastic with extensive nodularity
Residual disease	≤ 1.5 cm^2	≤ 1.5 cm^2	> 1.5 cm^2
Metastatic status	M0	M0	M1-M4

Abbreviations: IHC, immunohistochemistry

Table S3. Standard dose prescription for CNS tumours adapted from (1)

Tumour type	**Dose prescription/ fraction schedule**
Low grade glioma	50.4-54.0 Gy in 28-30 x 1.8 Gy
High grade glioma	54.0-59.4 Gy in 30-33 x 1.8 Gy
Ependymoma	50.1-59.4 Gy
Myxopapillary ependymoma	50.1 Gy in 30 x 1.67 Gy
Ependymoma WHO grade I and II	54.0 Gy in 30 x 1.8 Gy
Ependymoma WHO grade III	59.4 Gy in 33 x 1.8 Gy
Medulloblastoma low risk	Craniospinal: 18.0 Gy in 10 x 1.8 Gy Boost: 36 Gy in 20 x 1.8 Gy Total: 54.0 Gy in 30 x 1.8 Gy
Medulloblastoma standard risk	Craniospinal: 23.4 Gy in 13 x 1.8 Gy Boost: 30.6-32.4 Gy in 17-18 x 1.8 Gy Total: 54.0-55.8 Gy in 30-31 x 1.8 Gy
Medulloblastoma high risk	Craniospinal: 36.0 Gy in 20 x 1.8 Gy Boost: 18.0-19.8 Gy in 10-11 x 1.8 Gy Total: 54.0-55.8 Gy in 30-31 x 1.8 Gy
Non-metastatic AT/RT	54.0 Gy in 30 x 1.8 Gy
Metastatic AT/RT	Craniospinal: 36.0 Gy in 20 x 1.8 Gy Boost: 18.0 Gy in 10 x 1.8 Gy Total: 54.0 Gy in 30 x 1.8 Gy
Craniopharyngioma	50.4-54.0 Gy in 28-30 x 1.8 Gy
Neurocytoma	50.4-54.0 Gy in 28-30 x 1.8 Gy
Meningioma	50.1 Gy in 30 x 1.67 Gy

Abbreviations: CNS, central nervous system; AT/RT, atypical teratoid/rhabdoid tumour; Gy, Gray

Table S4. CTCAE v4.0 general guideline (13)

Grade	Criteria
1	Mild; asymptomatic or mild symptoms; clinical or diagnostic observations only; intervention not indicated
2	Moderate; minimal, local or non-invasive intervention indicated; limiting age-appropriate instrumental ADL
3	Severe or medically significant but not immediately life-threatening; hospitalization or prolongation of hospitalization indicated; disabling; limiting self-care ADL
4	Life-threatening consequences; urgent intervention indicated
5	Death related to AE

Abbreviations: CTCAE v4.0, Common Terminology Criteria for Adverse Events version 4.0; ADL, activities of daily living; AE, adverse event

Table S5. High-dose chemotherapy regimen administered in Fouladi et al. (29)

Timing	Chemotherapy
Day -4	Cisplatin 75 mg/m^2 and vincristine 1.5 mg/m^2 (maximum 2 mg); amifostine 600 mg/m^2 5 minutes before and 3 hours into cisplatin infusion
Day -3	Cyclophosphamide 2 g/m^2 IV over 1 hour, mesna by continuous infusion
Day -2	Cyclophosphamide 2 g/m^2 IV over 1 hour, mesna by continuous infusion
Day -1	Hydration after completion of chemotherapy
Day 0	Infusion of PBSC
Day +1	G-CSF 5 µg/kg/d SC daily until ANC > 2,000 µL for 2 consecutive days
Day +6	Vincristine 1.5 mg/m^2 (maximum 2 mg)

Repeat cycles every 4 weeks

NOTE. Four cycles of high-dose chemotherapy with PBSC support administered 6 weeks after completion of risk-adjusted craniospinal irradiation with conformal boost to the posterior fossa.

Abbreviations: IV, intravenously; PBSC, peripheral-blood stem cell; G-CSF, granulocyte colony-stimulating factor; SC, subcutaneously; ANC, absolute neutrophil count.